Analytic treatment of vortex states in cylindrical superconductors in applied axial magnetic field

A. Ludu,[1,2,a)] J. Van Deun,[3] M. V. Milošević,[1] A. Cuyt,[3] and F. M. Peeters[1]
[1]*Departement Fysica, Universiteit Antwerpen, Groenenborgerlaan 171, B-2020 Antwerpen, Belgium*
[2]*Department of Chemistry and Physics, Northwestern State University, Natchitoches, Louisiana 71497, USA*
[3]*Departement Wiskunde-Informatica, Universiteit Antwerpen, Middelheimlaan 1, B-2020 Antwerpen, Belgium*

(Received 14 May 2010; accepted 4 July 2010; published online 23 August 2010)

We solve the linear Ginzburg–Landau (GL) equation in the presence of a uniform magnetic field with cylindrical symmetry and we find analytic expressions for the eigenfunctions in terms of the confluent hypergeometric functions. The discrete spectrum results from an implicit equation associated to the boundary conditions and it is resolved in analytic form using the continued fractions formalism. We study the dependence of the spectrum and the eigenfunctions on the sample size and the surface conditions for solid and hollow cylindrical superconductors. Finally, the solutions of the nonlinear GL formalism are constructed as expansions in the linear GL eigenfunction basis and selected by minimization of the free energy. We present examples of vortex states and their energies for different samples in enhancing/suppressing superconductivity surroundings. © *2010 American Institute of Physics.* [doi:10.1063/1.3470767]

I. INTRODUCTION

The Ginzburg–Landau (GL) equation is a time-independent nonlinear magnetic Schrödinger equation that occurs in a variety of descriptions of macroscopical physical systems including deep water waves, nonlinear optics, pattern formation and filamentation, as well as in quantum confined systems such as superfluidity, Bose–Einstein condensation, and especially superconductivity.[1]

Modern lithography techniques enable the creation of very small superconducting structures of varied geometries.[2] The behavior of such *mesoscopic* structures in an external magnetic field is strongly influenced by the boundary conditions which in turn leads to new superconducting states.[3–5] In radially symmetric systems in the presence of axial magnetic field the superconducting state is characterized by a definite angular momentum which represents the number of flux quanta trapped by the sample. In systems of size comparable to the coherence length ξ, penetrating flux quanta are compressed into a single singularity of the wave function, called the "giant" vortex. In larger samples, the mutual vortex-vortex repulsion leads to a splitting of the giant vortex into a set of individual ones, called a multivortex state.[6,7] Experimentally, the distinction between the two allotropies of the state with the same vorticity can be made from the symmetry of the circulating Meissner currents, which is broken in the multivortex case.[8]

Besides quantum confinement, the presence of the boundary allows for another important physical phenomenon. When the sample is embedded in, e.g., a superconductor of higher critical temperature, one observes enhancement of superconductivity. This was shown in Refs. 9 and 10 for the disk and cylinder geometry. On the contrary, for a superconductor in a metallic medium, the leakage of Cooper-pairs leads to suppressed superconductivity at the boundary. Consequently,

[a)]Author to whom correspondence should be addressed. Electronic mail: ludua@nsula.edu.

in addition to the geometry dependence, we investigate in this paper the dependence of the vortex states (eigenvalues, linear basis, stability versus magnetic field) on the nature of the surrounding material.

As a necessary prerequisite for the full nonlinear approach, the construction of analytic solutions for the linear GL (LGL) equation is important because it expedites the understanding of various physical situations and limitations (like numerically unhandleable infinite or semi-infinite systems) and enables numerical calculations in the linear basis. Moreover, all nonlinear patterns and vortex structures can actually be obtained through linear combinations of the linear basis wave functions, while the full nonlinear approach basically just selects which of the solutions are (meta-)stable through minimization procedures.[11]

In this paper we investigate the GL equation in the order parameter Ψ of the Cooper-pair condensate placed in an axially symmetric magnetic field for fully three dimensional mesoscopic samples with cylindrical symmetry. Since recently, such superconducting samples (cylindrical wires and tubes) were experimentally realized.[12] We study the vortex states by expanding the solution of the nonlinear problem in the basis of *analytically obtained eigenfunctions* of the linear GL equation. Previous numerical investigations[6,7,13–15] of the full nonlinear GL problem were performed for thin disks and rings, where phase transitions between different superconducting states and between superconducting-normal state were studied using a self-consistent approach and the finite difference technique for solving two coupled GL equations.

The present paper is organized as follows. In Sec. II we investigate the dependence of the linear spectrum on the size of the cylinders and of the cavities. In Sec. III we analyze the LGL equation in terms of a Sturm–Liouville eigenfunction problem in cylindrical coordinates, and we find the fundamental set of linear solutions. Section IV gives the explicit analytic solution for solid cylindrical samples. In Sec. V we study the associated eigenvalue problem in terms of expansions in continued fractions. Finally, in Sec. VI, some interesting vortex states are constructed, and our findings are summarized in Sec. VII.

II. THEORETICAL FORMALISM

In what follows, we focus our attention in obtaining exact analytical solutions for the linear Ginzburg–Landau (LGL) treatment of a cylindrical mesoscopic superconducting sample in an axial uniform external magnetic field. We consider the superconducting order parameter to be a $C_2(\mathbf{R}_3)$ complex function $\Psi(\vec{r})$ defined inside the sample, as it describes the Cooper-pair density, also called *order parameter* (or simply wave function). As will be shown, an exact analytic solution of the LGL equation is a challenging task even in the case when uniform external field is present. In this paper, we solve the linear problem analytically and investigate the properties of its eigenfunctions and its spectrum.

We use the GL formalism in the limit of samples with size comparable or smaller than the magnetic field penetration depth λ, defined as the distance along which the magnetic field decays inside the superconductors (this characteristic length can be estimated[16] from the values of the phenomenological constants occurring in the free energy equation of the Ginzburg–Landau model of superconductivity, see below). Consequently, we may neglect the contribution to the Gibbs free energy due to the deformation of the magnetic field around the sample (following from the expulsion of magnetic flux[3,4]). In that case, the GL equation following from the minimization of energy with respect to Ψ is

$$\frac{1}{2m}\vec{P}^2\Psi + \alpha(T)\Psi + \beta|\Psi|^2\Psi = 0, \tag{1}$$

where the electromagnetic momentum operator $\vec{P}$ is given by

$$\vec{P} = -i\hbar\vec{\nabla} - \frac{q}{c}\vec{A}. \tag{2}$$

Here q, m are the charge and mass of the Cooper-pair, c is the speed of light in vacuum, and $\vec{A}$ denotes the vector potential of the applied magnetic field. The temperature dependent parameters

$$\alpha = \alpha_0\left(1 - \frac{T}{T_{c0}}\right), \quad \xi(T) = \frac{\hbar}{\sqrt{-2m\alpha(T)}}, \quad \xi_0 = \xi(0)$$

and the field penetration depth $\lambda^2 = -mc^2\beta/(16\pi q^2\alpha)$ (which is not explicitly used in this study) are given by the quantum statistical theory of superconducting phase transitions,[4,5,14] T_{c0} is the critical temperature in the absence of magnetic field. Usually, $\xi(T)$ is the coherence length (the characteristic length for the variation of the order parameter Ψ) and β is a constant in the neighborhood of interest for T around T_{c0}. The LGL equation is obtained from Eq. (1) by neglecting the nonlinear term with coefficient β, and it can be written as

$$\frac{1}{2m}\left(-i\hbar\vec{\nabla} - \frac{q}{c}\vec{A}\right)^2\Psi = -\alpha(T)\Psi. \tag{3}$$

The above equation for Ψ is fully applicable close to the superconducting/normal phase transition, where Ψ is small and the nonlinear term becomes indeed negligible. In order to write Eq. (3) in a compact form, we use the London electromagnetic gauge, $\nabla\cdot\vec{A} = 0$, and we renormalize the variables as

$$\vec{r} \to \vec{r}\frac{\sqrt{-2m\alpha(T)}}{\hbar}, \quad \vec{A} \to \vec{A}\frac{q}{(c\sqrt{-2m\alpha(T)})}, \quad \Psi \to \Psi\sqrt{-\frac{\beta}{\alpha(T)}}.$$

The LGL problem can now be written in dimensionless form as an eigenvalue problem for the operator

$$\hat{\mathcal{O}}\Psi = -\Delta\Psi + 2i\vec{A}\cdot\nabla\Psi + |\vec{A}|^2\Psi - \Psi = 0. \tag{4}$$

If the magnetic field has axial symmetry we can use cylindrical coordinates $\vec{r} \to (r, z, \varphi)$. In this case the azimuthal angle φ dependence in Eq. (4) can be separated, and $\hat{\mathcal{O}}$ has $\exp(iL\varphi)$ as eigenvalues labeled by the angular momentum L. This completely decomposes the space of solutions $\Psi(\vec{r})$ into orthogonal subspaces labeled by L (orthogonality is defined by the $L_2[0, 2\pi)$ norm),

$$\mathcal{L}^2(R^3) = \bigoplus_{L\in N} V_L, \quad V_L = \{\Psi/\Psi(\vec{r}) = \Phi(r,z)e^{iL\varphi}\}, \tag{5}$$

with $\Phi(r,z) \in \mathcal{L}^2(R^2)$ being a square integrable function. Decomposition of Eq. (5) reduces the problem to a two-dimensional one. On each of these subspaces the operator $\hat{\mathcal{O}}$ has a particular form depending on L, and for each such restricted operator we can attach an eigenvalue problem

$$\hat{\mathcal{O}}|_{V_L}\Phi_{\Lambda,\lambda} = \Lambda\Phi_{\Lambda,\lambda}, \tag{6}$$

where λ is a provisional degeneracy label, i.e., a quantum number. Of course, $\Lambda = \Lambda(L)$ and $\Phi_{\Lambda,\lambda}$ carry the L dependence. In what follows, we show that the range for Λ is determined by mapping the linear Ginzburg–Landau equation (1) into a Sturm–Liouville problem, and its values are in fact determined by the boundary conditions. In principle, we use this eigenvalue just as a parameter to label the linear eigenfunctions, together with L and λ. However, since $-\Lambda$ qualitatively substitutes the nonlinear term $\beta|\Psi|^2$ from Eq. (1), we expect for Λ to take physical reasonable values only in the range $[-1,0]$.

As a general rule for bounded mesoscopic superconductors in the presence of an uniform field, by expansion in Taylor series around $r\sim 0,\ z\sim 0$, we find that close to the center of the sample the linear solutions approach a confluent hypergeometric behavior. Close to the boundaries ($r\sim R,\ z\sim \pm h/2$), the solutions tend to acquire more singularities, and the LGL has a higher order of irregularity approaching a Heun function behavior.[17–19]

The operator in Eq. (4), called the Landau operator or the magnetic Schrödinger operator, is bound from below on the space of analytic functions on $\mathbf{R}_3$ independent of the nature of the magnetic vector potential $\vec{A}(\vec{r})$. This guarantees the existence of an energy spectrum bound from below.[20,21] In order to ensure the existence of a spectrum of real energies, some constraints should be applied on the vector potential. Namely, if the function $|\vec{A}|^4$ is integrable on $\mathbf{R}_3$, and $|\nabla\cdot\vec{A}|^2$ is also integrable (constraints which are automatically fulfilled by the London gauge), the Landau operator in Eq. (3) is self-adjoint (the Leinfelder–Simader theorem, based on Kato's inequality, see Ref. 20). Consequently, this operator always has a discrete component of its spectrum, bound from below, with eigenvalues Λ_n approaching $+\infty$ when $n\to+\infty$. The best example is given by Landau levels in a uniform magnetic field. Also, if the magnetic field $\vec{H}=\nabla\times\vec{A}$ decays to zero when $|\vec{r}|\to+\infty$, the spectrum is always positive, provided there are no limitations (boundary conditions) in the whole $\mathbf{R}_3$ space. This property is preserved even in the presence of an additional electric field, if the Coulombian potential fulfills certain constraints. Of course, the nature of the spectrum is always altered by the existence of boundary conditions. Note that depending on the asymptotic behavior of the magnetic field at infinity different types of spectrum can occur.[20,22–24]

In cylindrical coordinates the magnetic potential has the form

$$\vec{A}=\frac{\rho H}{2}\vec{e}_{\varphi},\quad H=\text{const},$$

and Eq. (6) becomes separable in (ρ,z). Its solutions can be written in the form

$$\Phi(\rho,z)=Q(\rho)(C_1\cos(\sqrt{\lambda}z)+C_2\sin(\sqrt{\lambda}z)), \tag{7}$$

where the radial part $Q(\rho)$ satisfies a Whittaker type of differential equation,[18,19]

$$-\frac{d^2Q}{d\rho^2}-\frac{1}{\rho}\frac{dQ}{d\rho}+\left(\frac{L^2}{\rho^2}+\frac{H^2\rho^2}{4}-(HL+\Lambda-\lambda+1)\right)Q=0. \tag{8}$$

Here λ [the degeneracy label from Eq. (6)] is the separation constant between the differential equations in ρ and z, and $C_{1,2}$ are arbitrary complex parameters to be determined from the boundary conditions.[25] This solution is the result of the standard procedure, as applied before in Refs. 4, 6, and 16. The fundamental set of solutions for Eq. (8) can be expressed in terms of linear combinations of Kummer (M) and Tricomi (U) confluent hypergeometric functions[26,27] as

$$Q_{L,\Lambda,\lambda}(\rho)=Q_0\rho^L e^{-H\rho^2/4}\Omega\left(\frac{1}{2}-\frac{\Lambda-\lambda+1}{2H},L+1;\frac{H\rho^2}{2}\right), \tag{9}$$

where $\Omega(c_1,c_2,\omega)=M(c_1,c_2,\omega)+CU(c_1,c_2;\omega)$, C is an arbitrary constant, and Q_0 is a normalization constant.[28] Similar solutions have been found for disks[6] and long cylinders[29] in a uniform field. Since the superconducting state develops when the mean value of the Landau operator becomes negative, we request the eigenvalue Λ to be nonpositive. The separation parameter λ that plays the role of a quantum number will become discrete after the application of boundary conditions. The three parameters L,Λ,λ form a complete set of quantum numbers for the LGL problem.

We associate the so-called modified Neumann boundary conditions to Eq. (6). This boundary condition (BC) requests for the superconducting current

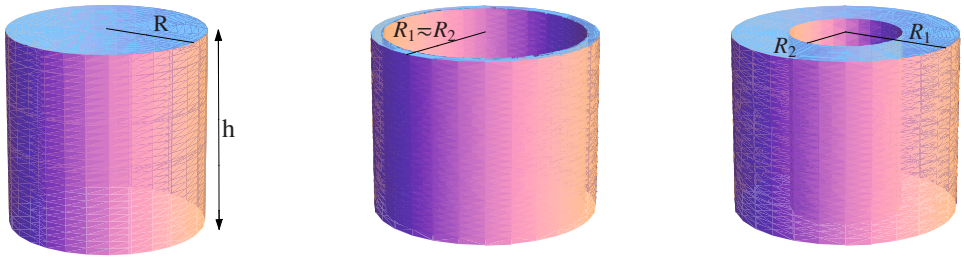

FIG. 1. (Color online) Considered superconducting geometries, (a) solid cylinders, (b) thin hollow cylinders $R \sim R_1 \sim R_2$, and (c) cylinders with a central hole $R_2 < R_1$. Inner radius (if any) is denoted by R_2 and outer one by R_1.

$$\vec{j} = q/(2m)(\Psi^* \vec{P}\Psi + (\vec{P}\Psi)^*\Psi)$$

to have a prescribed value at the surface of the sample, and the order parameter to have a smooth behavior at the origin (if inside the sample). In the case of samples in vacuum, we have the conventional Neumann BC for current, and regularity conditions for Φ, i.e.,

$$(\vec{n} \cdot \vec{P})\Phi|_\Sigma = 0, \quad |\Phi|_{|\vec{r}|=0,\infty} < +\infty. \tag{10}$$

Here Σ is the closed surface of the sample, and $\vec{n}$ is the normal to this surface (pointing out of the superconductor). In our formalism, we generalize the boundary condition to a mixed Dirichlet–Neumann condition, and we focus on surfaces of revolution for the samples, such that the surface Σ has cylindrical symmetry (as shown in Fig. 1). If the cylinder is solid, in order to satisfy the second condition in Eq. (10), we choose $C=0$ in Eq. (9), since the Tricomi function is singular at the origin. This is not the case, however, for cylindrical shells where we have to take into account both confluent hypergeometric functions.

In order to take into account the influence of a surrounding medium, we generalize the cylindrical boundary condition on Σ to a mixed Dirichlet–Neumann condition by assuming that in a narrow (of thickness b called the extrapolation length) external neighborhood of the surface Σ the order parameter has a simple exponential decay.[5,30] In uniform field, the normal component of the magnetic momentum operator reduces to the derivative with respect to the normal to the surface ($\vec{A}_n|_\Sigma = 0$). Therefore, we can write the boundary conditions in the form

$$\left(c_1 \frac{d\Phi}{d\vec{n}} + c_2 \Phi\right)_\Sigma = 0, \tag{11}$$

with $c_{1,2}$ as arbitrary constants. Actually, we can restrict the boundary coefficient constants (without loss of generality) to $c_2/c_1 = 1/b$, $b \in \mathbf{R}$. Parameter b takes the special physical value $b \to \pm\infty$ if the superconducting sample is placed in vacuum. If embedded in a superconducting material with higher critical temperature, which produces surface enhancement of superconductivity, we have $-\infty < b < 0$. Placed in a normal metallic material it will correspond to a surface suppression of superconductivity, $0 < b < \infty$, while in a ferromagnetic material we have $b=0$. Note that if the field and the boundary have the same symmetry, and the surface is smooth, the boundary conditions can be expressed just by keeping one of the coordinates constant, and let the other coordinates cover all of their ranges. If the surface is only piecewise smooth, the boundary conditions can still be expressed as above, but the other coordinates only cover disjoint intervals. If the boundary and the field have different symmetries, the boundary conditions cannot be written in a compact algebraic form, and various technical difficulties can occur related to the incompatibility of the boundary conditions and the functions in which the differential equation separates and can be integrated analytically.

III. MESOSCOPIC SUPERCONDUCTING SOLID CYLINDER

In this section, we study the case of a vertical solid cylinder of radius R and height h (pillars), in axial magnetic field, and surrounded by different materials described by different parameters b. The order parameter has the form given by Eqs. (7) and (9),

$$\Phi_{L,\Lambda,\lambda}(\rho,z)=\rho^{L}e^{-H\rho^{2}/4}M\left(\frac{1}{2}-\frac{\Lambda-\lambda+1}{2H},L+1;\frac{H\rho^{2}}{2}\right)(C_1\sin(\sqrt{\lambda}z)+C_2\cos(\sqrt{\lambda}z)). \tag{12}$$

The boundary conditions [Eq. (10)] take the form

$$\left.\frac{\partial\Phi}{\partial\rho}\right|_{\rho=R}=-\frac{1}{b_{lat}}\Phi(R,z),\quad z\in\left[-\frac{h}{2},\frac{h}{2}\right], \tag{13}$$

$$\left.\frac{\partial\Phi}{\partial z}\right|_{z=\pm h/2}=\mp\frac{1}{b_{\pm}}\Phi\left(\rho,\pm\frac{h}{2}\right),\quad \rho\in[0,R]. \tag{14}$$

Here we consider different surroundings for the lateral surface b_{lat}, for the upper b_+, and bottom lids b_-. The formalism can be equally used for blind cylindrical holes (cups) in materials, or cylindrical cavities, cases in which we simply change the sign in both right-hand sides of Eqs. (13) and (14), correspondingly. By applying the boundary condition on the top/bottom of the cylinder in Eqs. (13) and (14) we obtain a 2×2 system of homogeneous linear equations in $C_{1,2}$ whose solutions are nontrivial if the determinant is zero,

$$\begin{aligned}&\left(\sqrt{\lambda}\cos\frac{h\sqrt{\lambda}}{2}+\frac{1}{b_+}\sin\frac{h\sqrt{\lambda}}{2}\right)\left(\sqrt{\lambda}\sin\frac{h\sqrt{\lambda}}{2}-\frac{1}{b_-}\cos\frac{h\sqrt{\lambda}}{2}\right)\\&+\left(\sqrt{\lambda}\cos\frac{h\sqrt{\lambda}}{2}+\frac{1}{b_-}\sin\frac{h\sqrt{\lambda}}{2}\right)\left(\sqrt{\lambda}\sin\frac{h\sqrt{\lambda}}{2}-\frac{1}{b_+}\cos\frac{h\sqrt{\lambda}}{2}\right)=0.\end{aligned} \tag{15}$$

For all possible combinations of b coefficients we obtain from Eq. (15) a countable spectrum for the axial quantum number k, $\lambda\to\lambda_k$, $(C_{1,k},C_{2,k})$, where $k=0,1,2\ldots$, and the degenerate solution $\lambda_0=0$, $C_2=1$ when we have no z dependence of the order parameter (corresponding to flat disk or infinite long cylinder). An example of the axial excitation spectrum is presented in Fig. 2, where we plot λ_k versus b_+ curves, for several values of b_-, h. In the vacuum limit the eigenvalues have the asymptotic values from Eq. (17). The top/bottom surface enhancing/suppressing conditions can be compensated by height changes. Consequently, we have z-eigenvalue crossings for certain values of the parameters. Such level crossings induce degeneracy of the ground state, and hence transitions between different vortex configurations which otherwise are not favored energetically (no more adiabatic decoupling of such phases). For example, for $h=2\xi$ cylinder we have $\lambda_1(b_-=2)\sim\lambda_2(b_-=-5)$ when b_+ changes from -10 to 10.

In particular case when both top and bottom surfaces have similar conditions $(b_+=b_-=b)$ the coefficients fall in one of the two classes: z-asymmetric solutions with $C_1=1$, $C_2=0$ or z-symmetric solutions with $C_1=0$, $C_2=1$, with λ_k given by

$$\tan\frac{h\sqrt{\lambda}}{2}+(\sqrt{\lambda}b)^{\pm1}=0, \tag{16}$$

with $\pm$ for asymmetric/symmetric cases, respectively. In the simplest case when both ends are in vacuum $(b=\infty)$ we have the limiting z-quantization spectrum

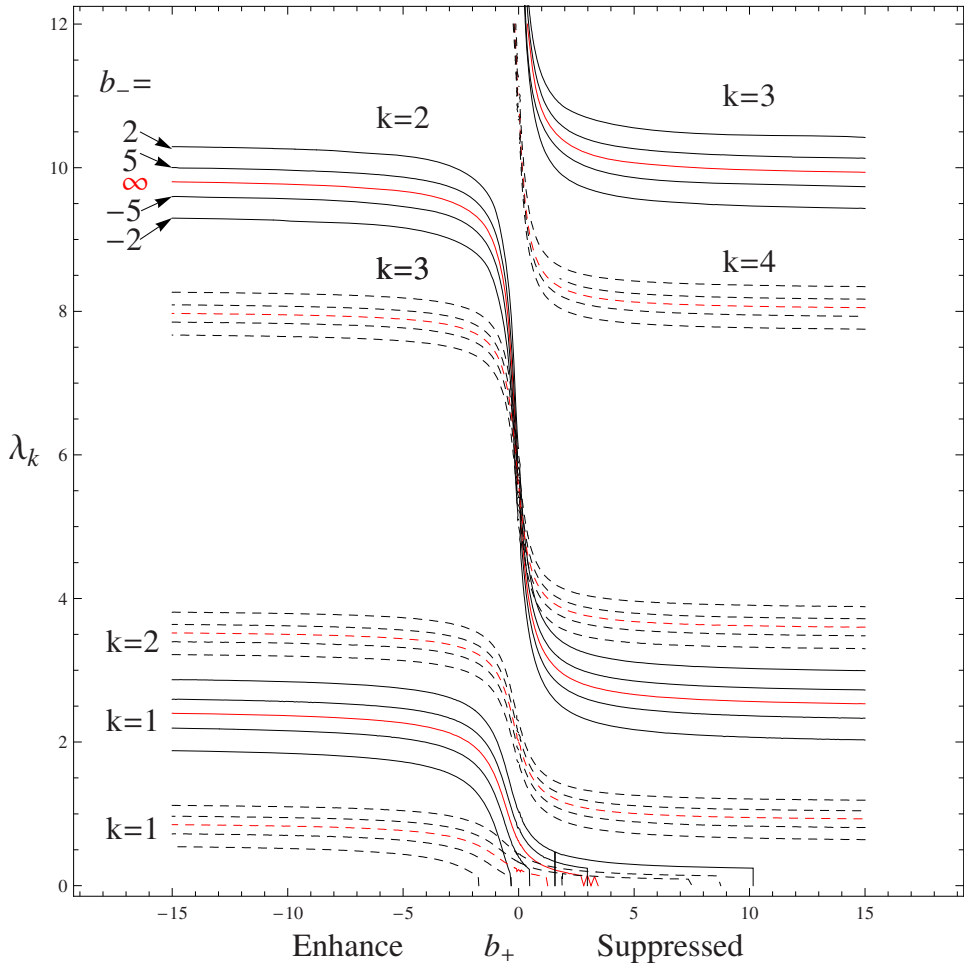

FIG. 2. (Color online) The axial excitation eigenvalues λ_k plotted vs the top surface superconductivity condition b_+ for solid cylinders of two different heights: $h=2\xi$ (solid lines) and $h=3.3\xi$ (dashed lines). Each set of five curves in a compact package represents different values for the surface conductivity at the bottom lid: $b_-=-5,-2,2,5$ (the four exterior curves of each package) and $b_-=\infty$ (vacuum: the middle curve of each package). For both surfaces in vacuum ($b_\pm=\infty$) the central curves of each package have asymptotic values $\lambda_k \to k^2\pi^2/h^2$. The z-quantum number k is written next to each package of eigenvalues for the two heights, respectively.

$$\lambda_{k,vac} = \frac{k^2\pi^2}{h^2}, \quad k = 0,1,\ldots . \tag{17}$$

The limiting values from Eq. (17) for λ_k are not only the vacuum limits, but they act as center lines for the eigenvalue bands whose spreading and position are controlled by the surface superconductivity conditions. In order to complete the fundamental solution in Eq. (12), we also have to solve Eq. (13) with respect to Λ. For solid cylinders we have

$$\left(L - \frac{HR^2}{2} - \frac{R}{b_{lat}}\right) M\left(\frac{1}{2} - \frac{\Lambda - \lambda_k + 1}{2H}, L+1, \frac{HR^2}{2}\right) + \frac{HR^2}{L+1}\left(\frac{1}{2} - \frac{\Lambda - \lambda_k + 1}{2H}\right) M\left(\frac{3}{2} - \frac{\Lambda - \lambda_k + 1}{2H}, L+2, \frac{HR^2}{2}\right) = 0, \tag{18}$$

with λ_k given by Eq. (15). This equation provides the eigenvalues of LGL problem for a superconducting cylinder in uniform magnetic field for a given set of parameters L, k, R, h, and H. Because of the oscillating behavior of the confluent hypergeometric series in Eq. (18), the solu-

tions for Λ form a countable set Λ_n, $n=0,1,\ldots$ bound from below [as predicted by the general spectral theory for the magnetic Schrödinger operator mentioned after Eq. (6) in Sec. II]. A new quantum number n must be added to the parameters and it is related to the radial excitations of the order parameter eigenfunction. We denote the final eigenvalues with $\Lambda_{L,k,n}(R,h,H) = \Lambda_{L,0,n}(R,h,H)+\lambda_k$, and we mention the additive contribution of the z-quantum number k to the Λ eigenvalues. Consequently, all axially excited states have larger values for Λ than the corresponding ground states. These states become less favored energetically as we show in Sec. V.

Going back to the "physical" meaning of the LGL spectrum, we note that the linear term $(\Lambda-\lambda)\Psi$ [see Eq. (8)] accounts for $|\Psi|^2\Psi$. Since the order parameter has the property $|\Psi|<1$, we consider for the nonlinear problem only those eigenvalues that fulfill $\Lambda_{L,k,n}(R,h,H)<\lambda_k$, which brings a restriction to the upper bound of this spectrum.

The qualitative properties of the $\Lambda_{L,k,n}$ spectrum obtained in Eq. (18) for a solid cylinder of radius R can be understood if we map the differential equation, Eq. (8), together with the BC given in Eq. (10), into the self-adjoint form

$$L[Q] = \Lambda q(\rho) Q, \tag{19}$$

with

$$L[Q] = -\frac{d}{d\tilde{\rho}}\left(p(\tilde{\rho})\frac{dQ}{d\tilde{\rho}}\right) + \left(\frac{L^2}{\tilde{\rho}^3} + \frac{H^2\tilde{\rho}}{4} - \frac{HL+1}{\tilde{\rho}}\right), \tag{20a}$$

$$r(\tilde{\rho}) = R^2\tilde{\rho}, \quad q(\tilde{\rho}) = \frac{1}{\tilde{\rho}}. \tag{20b}$$

In this form we have $\tilde{\rho}=\rho/R \in (0,1]$ with $p(\tilde{\rho})>0$ and $q(\tilde{\rho})>0$. The system equation (19) shows that the radial differential equation in Eq. (8) and its BC in Eq. (10) form a regular Sturm–Liouville problem.[31] From the general theory of the Sturm–Liouville two-point boundary value problem we know that all eigenvalues Λ are real and form a semi-infinite sequence bounded from below $\Lambda_{L,0,0}<\Lambda_{L,k,n}<\cdots<\Lambda_{L,k',n'}$ if $0<n<n'$, $0<k<k'$. According to the physical restriction $\Lambda<\lambda$ established earlier, the spectrum of physical interest is discrete and bounded. None of the eigenvalues $\Lambda_{L,k,n}$ are degenerate, and to each two distinct eigenvalues correspond two linear independent eigenfunctions, orthogonal with respect to the weighed scalar product. As a result, for given L, and a given solid cylinder of radius R, if $k_1\neq k_2$, and/or $n_1\neq n_2$, we have

$$\langle Q_{L,k_1,n_1}, Q_{L,k_2,n_2}\rangle = \frac{R^2}{2}\int_0^R \rho^2 Q_{L,k_1,n_1} Q^*_{L,k_2,n_2} d\rho = 0. \tag{21}$$

Normalized with respect to the weight $r(\rho)$, the eigenfunctions form a complete orthonormal basis of piecewise continuous functions, with piecewise square integrable continuous derivative in $\rho \in [0,R]$.

As a general check, we write Eq. (18) in the limit $R\to\infty$. By using the asymptotic expansion

$$Q(\rho) \sim L!R^L e^{-HR^2/4}\left[\frac{\left(\frac{HR^2}{2}\right)^{\Lambda/2H}}{\Gamma\left(L+1+\frac{\Lambda}{2H}\right)} + \frac{e^{HR^2/2}\left(\frac{HR^2}{2}\right)^{-(\Lambda/2H)-L-1}}{\Gamma\left(-\frac{\Lambda}{2H}\right)}\right], \tag{22}$$

we reobtain the Landau levels

$$\Lambda_{L,k,n} \to H(2L+2n+3)-2, \tag{23}$$

as expected for an infinite space.

IV. ENERGY SPECTRUM IN TERMS OF CONTINUED FRACTIONS

In order to have an efficient handling of the BC equation (18) through an analytical approximation for Λ, we use continued fractions[32] as the best available approximation of the confluent hypergeometric functions occurring in the order parameter expressions. We rewrite Eq. (18) as

$$\Lambda = C \cdot K(\Lambda) + H + \lambda_k - 1, \tag{24}$$

where the constant C is given by

$$C = \frac{(L+1)}{R^2}\left(L - \frac{HR^2}{2} - \frac{R}{b_{lat}}\right) \tag{25}$$

and

$$K(\Lambda) = \frac{M\left(\frac{1}{2} - \frac{\Lambda - \lambda_k + 1}{2H}, L+1, \frac{HR^2}{2}\right)}{M\left(\frac{3}{2} - \frac{\Lambda - \lambda_k + 1}{2H}, L+2, \frac{HR^2}{2}\right)}.$$

Writing $\eta = HR^2/2 - R/b_{lat}$ we use formula (16.1.13a) from Ref. 32 to obtain a continued fraction expansion for the function $K(\Lambda)$,

$$K(\Lambda) = 1 + \cfrac{a_1\eta}{1 + \cfrac{a_2\eta}{1 + \cfrac{a_3\eta}{1 + \ddots}}}, \tag{26}$$

where the coefficients a_n are given by

$$a_{2n+1} = \frac{-\left(L + 1 + \frac{3}{2} - \frac{\Lambda - \lambda_k + 1}{2H} + n\right)}{(L+1+2n)(L+2+2n)},$$

$$a_{2n} = \frac{\frac{1}{2} - \frac{\Lambda - \lambda_k + 1}{2H} + n}{(L+2n)(L+1+2n)}. \tag{27}$$

Taking an even contraction[32] of this fraction gives

$$K(\Lambda) = 1 + K_{m=1}^{\infty}\frac{c_m}{d_m},$$

where $c_1 = a_1 z$, $d_1 = a_2 z + 1$, $c_m = -a_{2m-2}a_{2m-1}z^2$, and $d_m = a_{2m}z + 1 + a_{2m-1}z$. If we denote the kth approximant by $A_k(\Lambda)/B_k(\Lambda)$, then Eq. (24) becomes

$$p_k(\Lambda) = CA_k(\Lambda) - \Lambda B_k(\Lambda) = 0,$$

where p_k is a polynomial of degree $k+1$, which satisfies the recurrence relation[32]

$$p_k = d_k p_{k-1} + c_k p_{k-2} = (1 + a_{2k}z + a_{2k-1}z)p_{k-1} - a_{2k-2}za_{2k-1}zp_{k-2}$$

for $k \geq 2$. The formulas for $k=1$ and $k=0$ are somewhat different but we omit the details here. Defining

$$P_k = \frac{1}{L+2k+2} \cdot \frac{p_k}{(-a_{2k+1}z)(-a_{2k-1}z)\cdots(-a_3z)(-a_1z)}$$

gives the recurrence relation written as a product of matrices

$$\begin{bmatrix} \frac{k-1}{L+2k-1} & \frac{L+2k}{z}+\frac{k}{L+2k+1}-\frac{L+k}{L+2k-1} & -\frac{L+k+1}{L+2k+1} \end{bmatrix} \begin{bmatrix} P_{k-2}(\Lambda) \\ P_{k-1}(\Lambda) \\ P_k(\Lambda) \end{bmatrix}$$
$$= \frac{\Lambda}{2H} \begin{bmatrix} \frac{1}{L+2k-1} & \frac{1}{L+2k+1}+\frac{1}{L+2k-1} & \frac{1}{L+2k+1} \end{bmatrix} \begin{bmatrix} P_{k-2}(\Lambda) \\ P_{k-1}(\Lambda) \\ P_k(\Lambda) \end{bmatrix}.$$

Note that $P_k(\Lambda)$ is a rational function of Λ that has the same zeros as the polynomial $p_k(\Lambda)$. Writing down this recurrence relation for $k=0,\ldots,n-1$, collecting in matrices, and filling in a zero of p_{n-1} for Λ, leads to the generalized eigenvalue problem

$$\mathcal{A}_n \vec{P}_n = \Lambda \mathcal{B}_n \vec{P}_n,$$

where the matrices $\mathcal{A}_n$ and $\mathcal{B}_n$ are given by the general form

$$\mathcal{A}_n = \begin{bmatrix} \frac{L}{z} & -1 & & & & \\ -\frac{L}{z} & \frac{L+2}{z}+\frac{1}{L+3} & -\frac{L+3}{L+5} & & & \\ & \frac{1}{L+3} & \ddots & \ddots & & \\ & & \frac{L+2n-4}{z}+\frac{n-2}{L+2n-3}-\frac{L+n-2}{L+2n-5} & -\frac{L+n-1}{L+2n-3} & & \\ & & \frac{n-2}{L+2n-3} & \frac{L+2n-2}{z}+\frac{n-1}{L+2n-1}-\frac{L+n-1}{L+2n-3} \end{bmatrix}, \tag{28}$$

$$\mathcal{B}_n = \frac{1}{2H} \begin{bmatrix} \frac{2HL}{zC} & \frac{1}{L+1} & & & & \\ 0 & \frac{1}{L+3} & \frac{1}{L+3} & & & \\ & \frac{1}{L+3} & \frac{1}{L+3}+\frac{1}{L+5} & \frac{1}{L+5} & & \\ & & \ddots & \ddots & \ddots & \\ & & & \frac{1}{L+2n-5} & \frac{1}{L+2n-5}+\frac{1}{L+2n-3} & \frac{1}{L+2n-3} \\ & & & & \frac{1}{L+2n-3} & \frac{1}{L+2n-3}+\frac{1}{L+2n-1} \end{bmatrix}.$$

The first two lines in these matrices correspond to cases $k=0$ and $k=1$, for which the recurrence formulas are a little different from the general case, as mentioned above. The n eigenvalues correspond exactly to the n zeros of p_{n-1}. If $n\to\infty$ then the eigenvalues converge to the solutions of Eq. (24). This equation has infinitely many solutions, but the solutions near zero will be found first.

To study the occurrence of negative solutions in Eq. (24), we reason as follows. Using the Kummer transformation[27]

$$M(a,b,z) = e^z M(b-a,b,-z)$$

and the asymptotic formula[27]

$$M(a,b,z) \sim \Gamma(b) e^{z/2} \left(\frac{1}{2}bz - az\right)^{1/4-b/2} \pi^{-1/2} \cos\left(\sqrt{2bz-4az} - \frac{1}{2}b\pi + \frac{\pi}{4}\right)$$

for $a\to-\infty$ and z real, computations yield

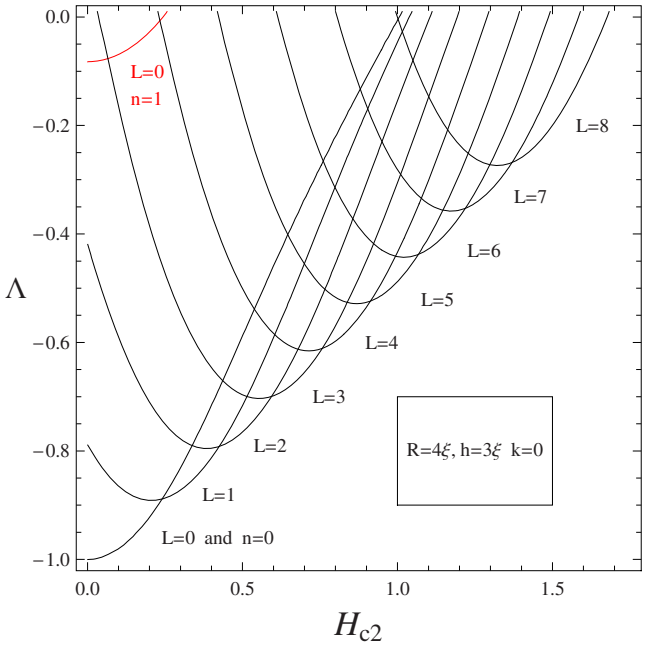

FIG. 3. (Color online) Lowest-energy spectra $\Lambda_{L,k=0,n=0}(H,L)$ dependence on the reduced magnetic field H/H_{c2} for a cylinder of radius $R=4\xi$ and height $h=3\xi$, $L\leq 8$. For different Ls the eigenvalue minima line up. One radially excited level ($L=0$, $n=1$, $k=0$) occurs in this range for Λ (left top corner).

$$K(\Lambda)\sim\frac{R}{2(L+1)}\left(\sqrt{-\Lambda}-\frac{HR}{2}\right),\quad \Lambda\to-\infty,$$

where we used some basic trigonometric identities and the fact that $\cos(a+ib)=\cos(a)\cosh(b)-i\sin(a)\sinh(b)$ and similarly for the sine. Furthermore, it follows immediately from the definition of M as a power series that $K(\Lambda)>0$ for $\Lambda\leq 0$ (because in that case all terms in the series are positive). So if $C>0$ then Eq. (24) can never have a negative solution. On the other hand, if $C<0$ we have

$$C\cdot K(\Lambda)<\Lambda,\quad \Lambda=0,$$

$$C\cdot K(\Lambda)>\Lambda,\quad \Lambda\to-\infty,$$

and Eq. (24) must have at least one negative solution. Equation (27) provides an excellent approximation of the linear spectrum for a superconducting cylinder.

We present in Fig. 3 a generic aspect of the linear spectrum for a solid cylinder $R=4\xi$, $h=3\xi$, obtained with Eq. (24), for the ground state ($n=k=0$) and one radially excited state ($n=1$). For different L values the eigenvalue minima align toward an asymptotic direction given by the corresponding Landau levels. In Figs. 4 and 5 we show a comparison between the eigenvalues obtained for different excited states $n\neq 0$ and/or $k\neq 0$.

By construction, the z-excitations $k>0$ just add a constant (H-independent) term to the $k=0$ ground states. The boundary conditions can be rewritten for the special cases of thin disks or very long cylinders. This can be explained by the fact that for $R\gg h$ the confluent hypergeometric series approaches[27]

$$M(a,b,z)\to\Gamma(b)\left(\frac{e^z z^{a-b}}{\Gamma(a)}+\frac{z^{-a}}{\Gamma(b-a)}\right),$$

and Eq. (18) reduces to

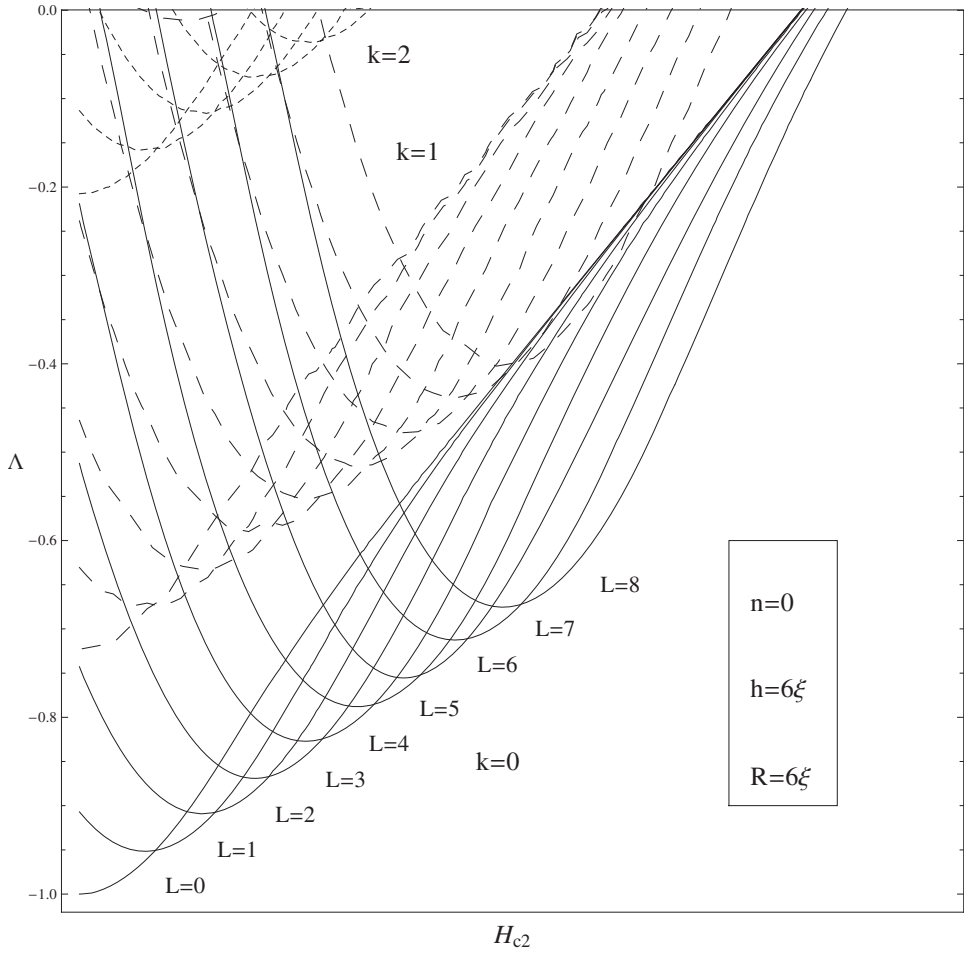

FIG. 4. Axial excited states and ground state $\Lambda(H)$ for a solid cylinder of height $h=6\xi$ and radius $R=6\xi$ for different values for the z-quantum number: $k=0$ (solid line), $k=1$ (dashed line), and $k=2$ (dotted line) for same $n=0$ radial quantum number and $L=0,\ldots,8$

$$\Lambda_{L,k,n} \to -2HL - 2H(n+1) - \lambda_k - 1,$$

showing an increase in the density of eigenvalues. In the $h/R \to 0$ limit, the spectrum shows a linear degeneration on top of Landau levels. On the contrary, when the ratio h/R increases the spectrum becomes sparser and the eigenvalues approach larger numbers. In Fig. 6 we present the dependence of the linear spectrum for fixed L and H as a function of the h/R ratio. For larger values of the radius the spectrum can be approximated by the expression

$$\Lambda_{L,k,0} \to H(2L+1) - 1 + \frac{k^2\pi^2}{h^2}. \tag{29}$$

We show the dependence on R of the eigenvalues for different radial quantum numbers n in Fig. 7. We found that the energy exhibits minimum at a finite R, and that minimum shifts toward larger radii for larger n. In addition, for $R > 3\xi \sim h$ the spectrum virtually does not change with R and converges to our derived expression of Eq. (29).

With the analytical expressions for the eigenvalues $\Lambda_{L,k,n}(H,R,h,b)$, we can calculate the radial-dependent part of the wave function $Q(\rho)$. For example, in the $L=0$ state the absolute value of the wave function is minimum at the cylinder's edges where the applied magnetic field begins to diffuse into the sample (Fig. 8). For $L \neq 0$ the wave function has a zero on the axis, followed by

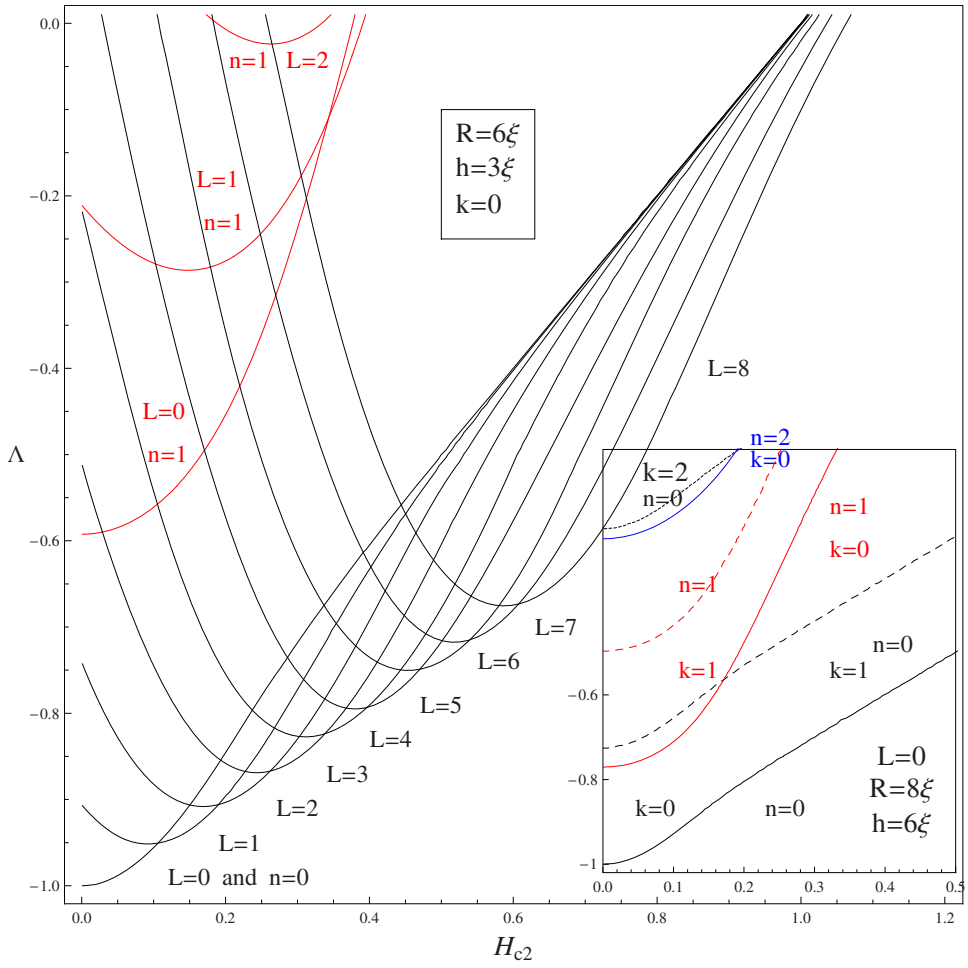

FIG. 5. (Color online) Radial excited states and ground state for same cylinder in Fig. 4. Radial quantum number $n=0$ (the nine bottom curves) and $n=1$ (the three upper curves) for $k=0$, $L=0,\ldots,8$. For comparison, in the small window we present several $L=0$ states for a $R=8\xi$ cylinder for some values for n,k.

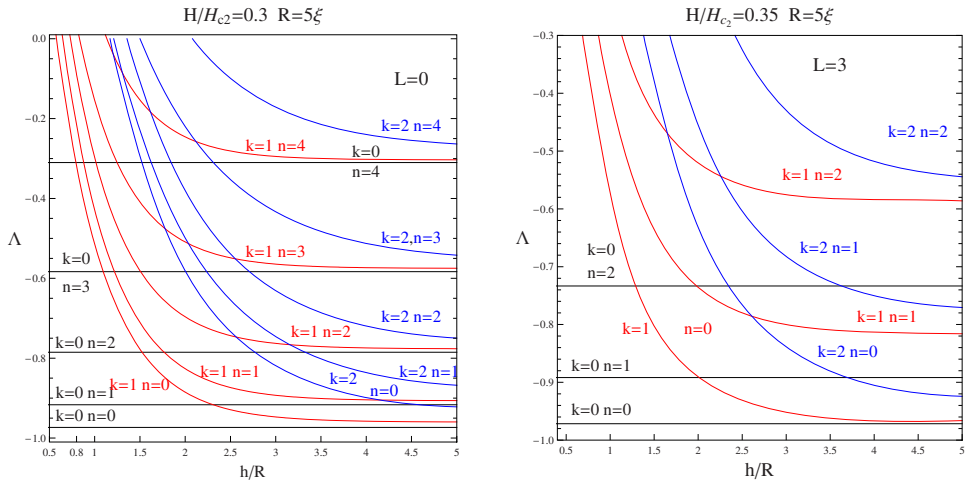

FIG. 6. (Color online) Dependence of the cylinder eigenvalues Λ vs the ratios h/R for $n=0,\ldots,4$, $k=0$, $k=1$, and $k=2$. Left frame: $L=0$, $H/H_{c_2}=0.2$. Right frame: $L=3$, $H/H_{c_2}=0.3$. Evidently, ground states do not depend on h. All excited states (nonhorizontal lines) approach asymptotically the corresponding ground state in the limit of long cylinder and disappear in the limit of flat disks.

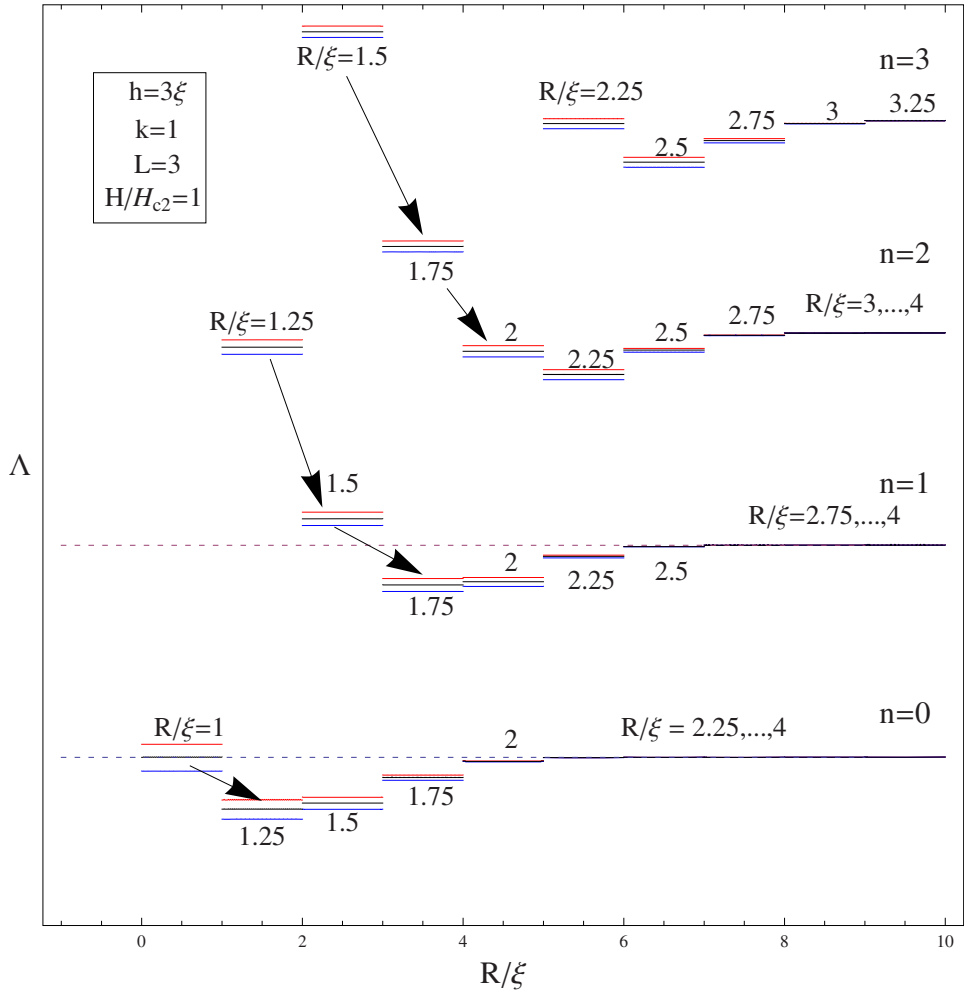

FIG. 7. (Color online) Dependence of Λ for the ground state ($k=0$, $n=0$) and three excited radial states ($n=1,2,3$ and $k=0$) vs the radius of the cylinder in the range $R=\xi\div 4\xi$. We plot eigenvalues for three different surrounding materials: $b=\infty$ (vacuum, center lines of each triplet), $b=5$ (surface suppressing superconductivity, upper lines of each triplet), and $b=-5$ (surface enhancing superconductivity, lowest lines of each triplet). The dotted line represents the approximation from Eq. (29).

a local minimum toward the cylinder's edge (analogous to $L=0$ case). Increasing magnetic field suppresses further the wave function at the edge. More examples for the dependence of the order parameter $\Phi(\rho,z=0)$ versus the radial coordinate are presented in Fig. 9.

We note a direct consequence on the linear spectrum, occurring from the generic linear eigenvalue problem, and the associated boundary conditions. If we write Eq. (8) in the elliptic normal form

$$\frac{\partial}{\partial\rho}\left(\rho\frac{\partial\Phi}{\partial\rho}\right)+\frac{\partial}{\partial z}\left(\rho\frac{\partial\Phi}{\partial z}\right)+\gamma(\rho)\Phi=0, \tag{30}$$

and use the Rayleigh quotient theorem,[21] Eq. (30) provides stable eigenstates $\Phi(\rho,z)$ for satisfied inequality

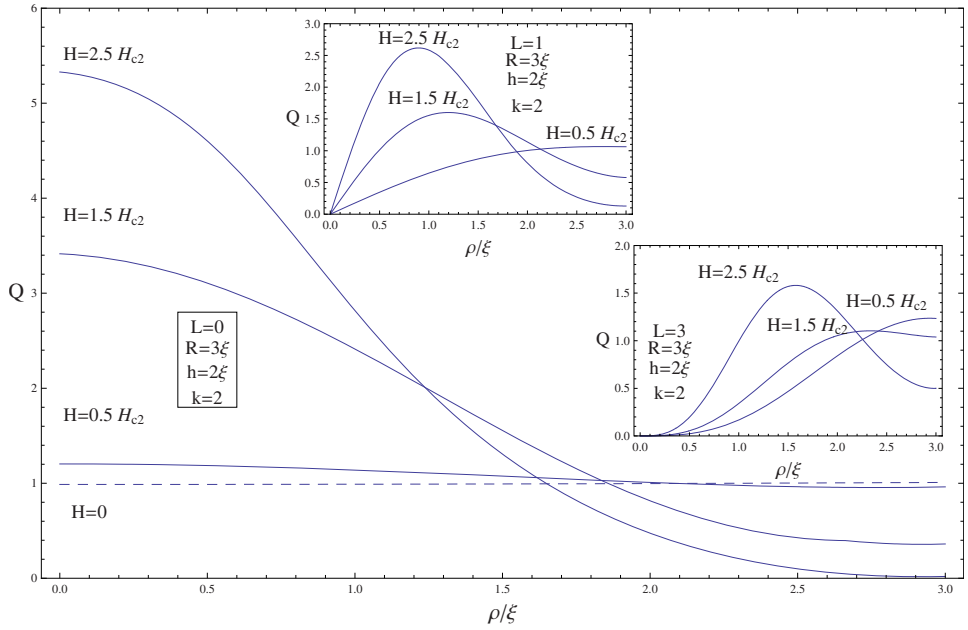

FIG. 8. (Color online) The radial part of the order parameter for a superconducting cylinder for different values of magnetic field (H=0.5,1.5,2.5) and angular momentum (L=0,1,3).

$$\gamma(\rho) = \rho\left(-\frac{L^2}{\rho^2} - \frac{H^2\rho^2}{4} + HL + \Lambda - \lambda_k + 1\right) \leq 0, \tag{31}$$

which is obtained from one of the Rayleigh quotient conditions of stability (the rest of stability conditions are fulfilled by the chosen boundary conditions). This condition provides strict limitations concerning the region where the superconducting state can exist. Namely, the superconducting state [nonzero $\Phi(\rho,z)$] survives only within the range of ρ enclosed between the two real roots of Eq. (31). From Fig. 10 we notice that the cylindrical superconducting domain narrows down with increasing magnetic field and increasing vorticity because the superconducting state is imploded by the increasing external magnetic field. For L=0 the superconducting zone is confined at the cylinder axis, but for $L>0$ the superconducting state is stable in a cylindrical layer between the central vortex and the external surface.

In the following we present the z-dependence of the superconducting order parameter. In Figs. 11 and 12 we present the wave function plotted in the (ρ,z) plane, for the L=0 and L=1 states, for the combinations of (n,k) quantum numbers providing the lowest energy states (the ground state and first two excited states). In the Meissner phase and n=k=0, superconductivity is more sup-

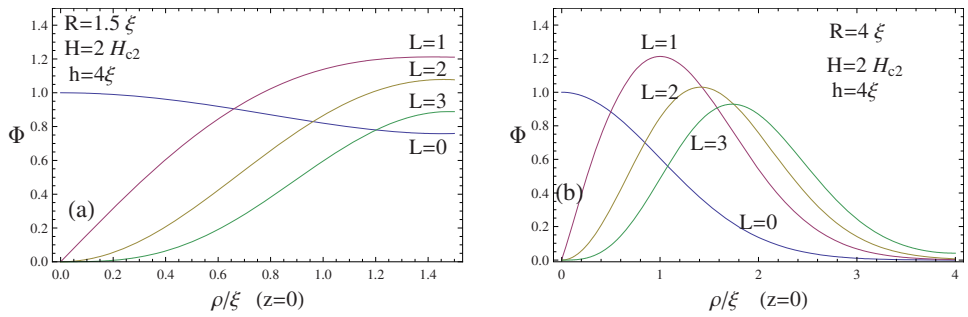

FIG. 9. (Color online) The superconducting order parameter $\Phi(\rho,z=0)$ for a cylinder of height h=4ξ and radii (a) R =1.5ξ and (b) R=4ξ for the ground-state (k=n=0) and angular momenta L=0–3.

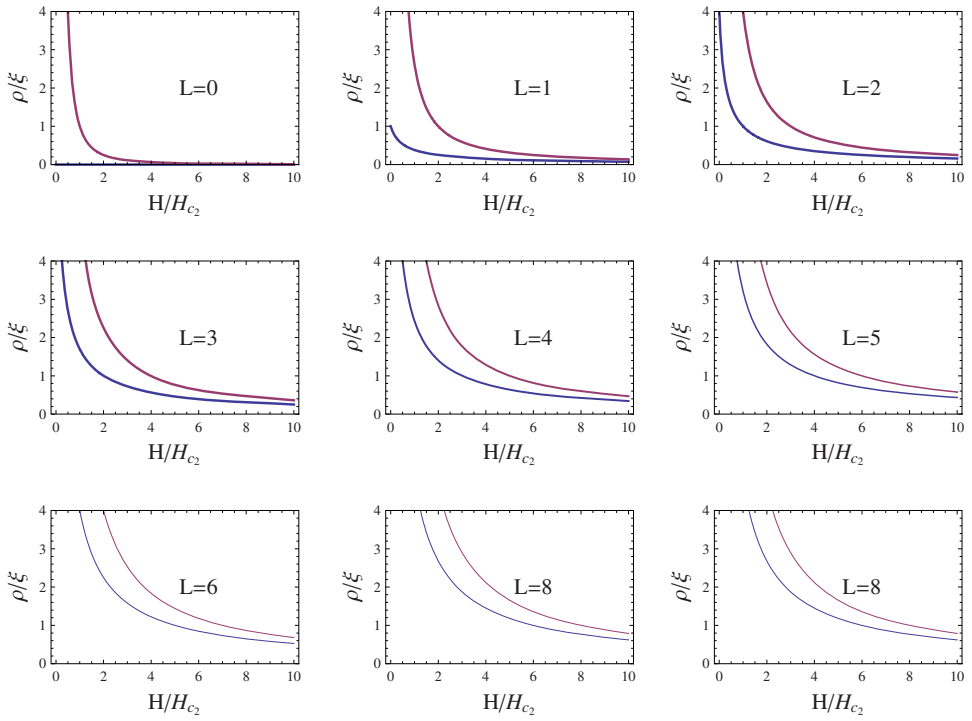

FIG. 10. (Color online) The region between the two curves corresponds to the radial range for the existence of the superconducting state which is shown for different angular momentum. For a cylinder of radius $R=4\xi$, height $h=8\xi$ and ground states $n=k=0$.

pressed at the edges of the bases of the cylinder than in the equatorial plane. In the first excited state $(n=0,\ k=1)$, the zero-order-parameter plane is formed in the sample at $z=0$. With further increasing quantum number k, more $\Psi=0$ planes nucleate in the sample (for $k=1$, two more planes appear at $z=\pm h/4$). In an analogous fashion, increased radial quantum number n induces zero-order-parameter concentric rings. Combinatorial (n,k) values sample the cylinder into $2k(n+1)$ ring-like superconducting segments.

V. CONSTRUCTION OF VORTEX STATES FOR A SOLID CYLINDER

The eigenvalues Λ and corresponding eigenfunctions found for given angular momentum in Sec. IV directly determine the free energy $\mathcal{F}$ of the giant vortex states, where now the previously omitted nonlinear GL term can be *included*. After minimization of the energy with respect to the normalization constant, one obtains for the superconducting order parameter of the vortex state for chosen quantum numbers (n,k) (see Ref. 9)

$$\psi(\rho,z)=\left(-\Lambda_{L,k,n}\frac{I_2}{I_1}\right)^{1/2}\Phi_{L,\Lambda_{L,k,n},k}(\rho,z)e^{iL\varphi}, \tag{32}$$

and the minimized energy of that vortex state is

$$\mathcal{F}=-\Lambda_{L,k,n}^2\frac{I_2^2}{I_1}, \tag{33}$$

where

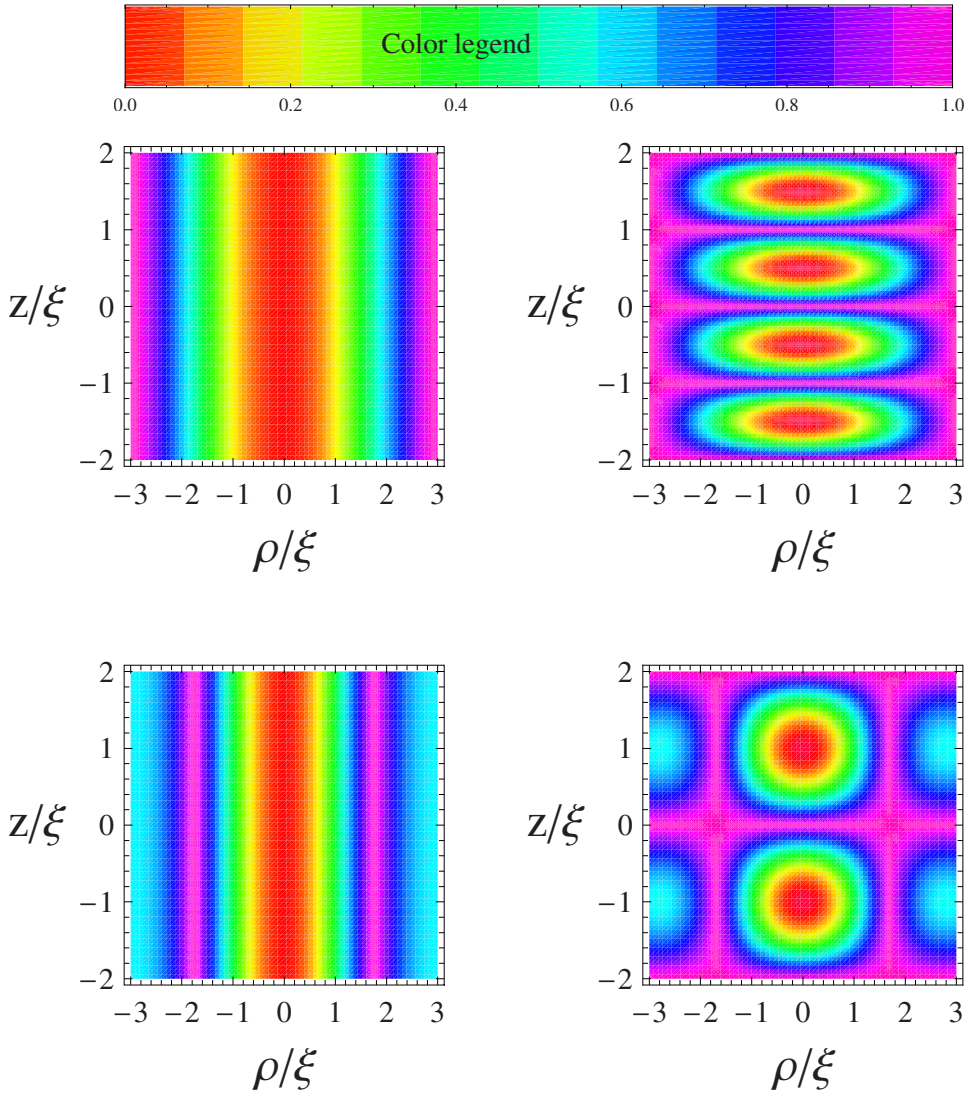

FIG. 11. (Color online) The order parameter for a cylinder of radius $R=3\xi$ and height $h=2\xi$ for $H=0.5H_{c2}$ and $L=0$. Contour plots of the ground state and excited states. The vertical axis corresponds to the direction of the applied magnetic field.

$$I_1=\int_{-h/2}^{h/2}\int_0^R \rho\Phi^4_{L,\Lambda_{L,k,n},k}(\rho,z)d\rho dz, \quad I_2=\int_{-h/2}^{h/2}\int_0^R \rho\Phi^2_{L,\Lambda_{L,k,n},k}(\rho,z)d\rho dz.$$

In Fig. 13 the Gibbs free energy is plotted against magnetic field intensity for a solid cylinder ($R=3\xi$, $h=2\xi$) in vacuum ($b=1000$), for eigenstates $\Phi_{L,\Lambda_{L,k,n},k}(\rho,z)\exp(iL\varphi)=\Phi_{L,k,n}\exp(iL\varphi)$ of different vorticities $L=0,1,\ldots,6$ for the ground and first excited states, calculated with Eq. (33). We stress here that the dependence of the free energy-magnetic field-vorticity profiles on the axial excitations has a very simple additive expression. Moreover, the dependence of these curves on the nature of the surrounding material (the dependence on the b parameter) is very simple and almost linear.

The GV states (giant vortex) are constructed solely with one such eigenstate, except that the domain of definition for the field is restricted by the stability criterion for the normalized $\Lambda\in[-1,0]$. In Fig. 14 we study the influence of the radius of the solid cylinder on the magnetic field and vorticity dependence of the free energy for two different surface conditions. We notice

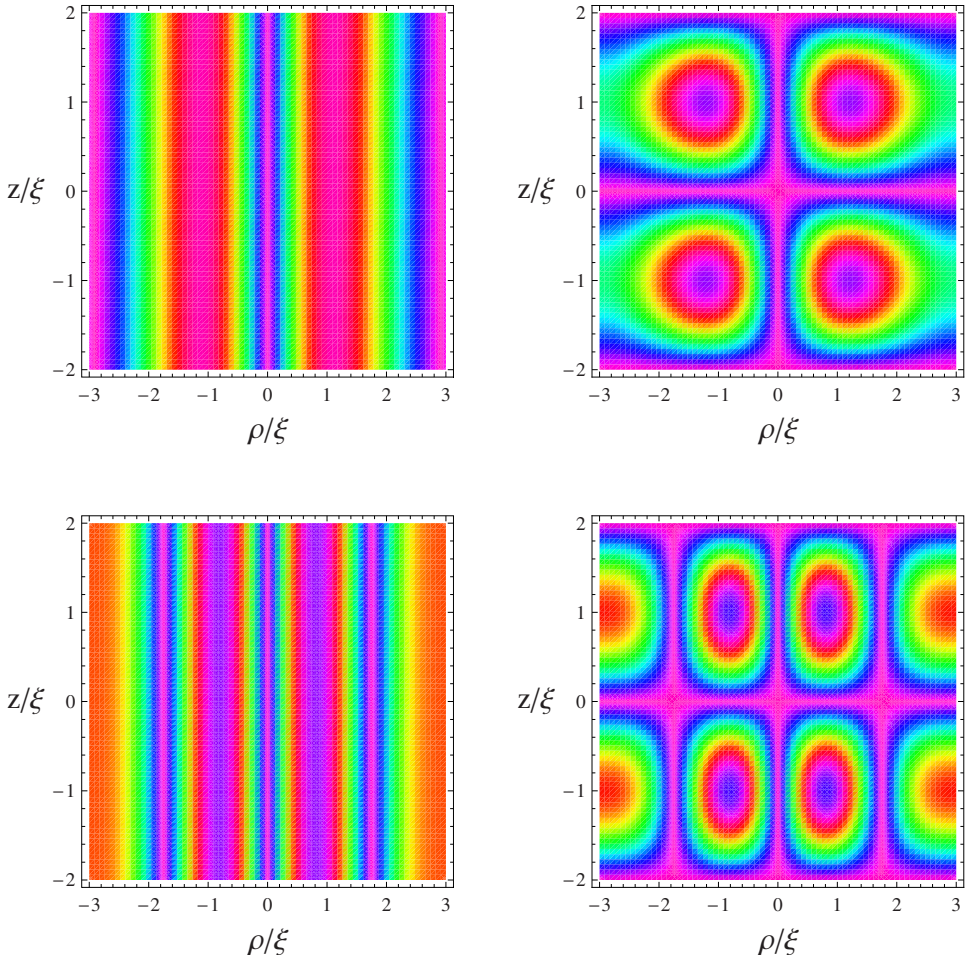

FIG. 12. (Color online) The order parameter for a cylinder of radius $R=3\xi$ and height $h=2\xi$, for $H=1.5H_{c2}$ and $L=1$, plotted in the (ρ,z) plane for the ground state and the excited states.

that the aspect of the family of free energy versus magnetic field can be influenced by the radius very much for suppressed superconducting surface, especially at lower fields. In Fig. 15 we show the behavior of the free energy as a function of the magnetic field, for different vorticity of the vortex state, and for modified boundary conditions at the sample surface, and that for cylinders with two different radii. The boundary condition corresponding to a surrounding normal metal ($b>0$), and the proximity effect, i.e., leakage of the Cooper-pairs, suppresses superconductivity. Vice versa, superconductivity is enhanced by $b<0$, and that is visible through the large critical field of the superconducting state for the corresponding curves in Fig. 15, and the number of vortices fitting the sample at that field. We also note that the influence of the surface on the stability of GV structures is stronger in thinner cylinders. For same values of b taken for the larger cylinder as for the smaller one, the maximal vorticity and critical field of the states are virtually unaffected, contrary to the situation in the thin sample.

In order to construct the states that break the cylindrical symmetry (so-called multivortex states), we linearly expand the nonlinear order parameter in the basis of LGL eigenfunctions as

$$\psi(\rho,\varphi,z)=\sum_{L_j} C_j \Phi_{L_j,k,n}(\rho,z)\exp(iL_j\varphi), \tag{34}$$

and minimize the energy with respect to the complex coefficients C_j.

When we limit ourselves to only two LGL eigenfunctions, the free energy can be expressed as

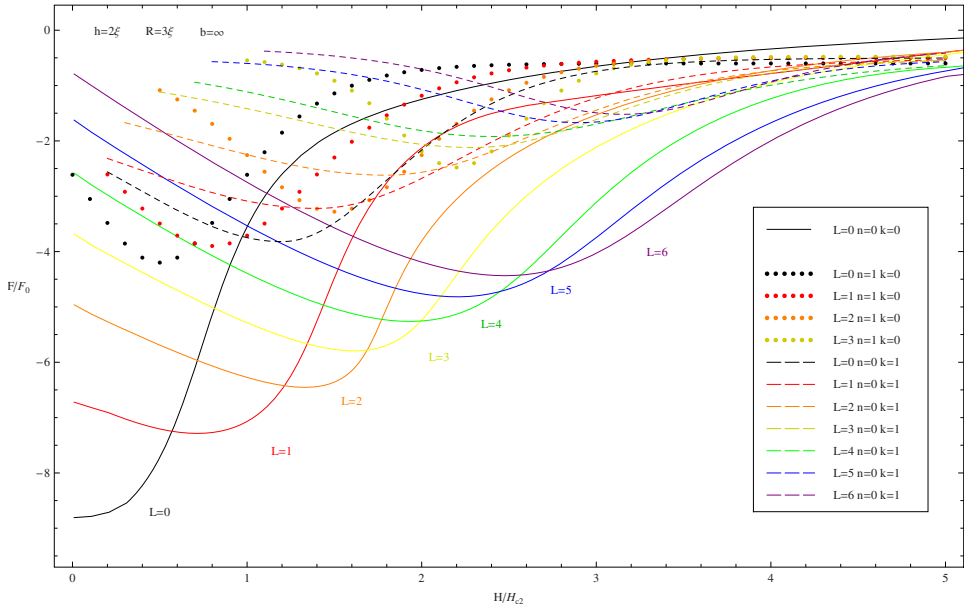

FIG. 13. (Color online) The Gibbs free energy vs the applied magnetic field plot for a solid cylinder ($R=3\xi$, $h=2\xi$) in vacuum ($b=\infty$) for eigenstates $\Phi_{L,n,k}(\rho,z)\exp(iL\varphi)$ of different vorticities. Solid lines represent ground energy states ($n=0$, $k=0$). For fixed L value the dotted curves represent excited states ($n=1$, $k=0$), and dashed curves represent excited states ($n=0$, $k=1$).

$$\mathcal{F}=C_1^4A_1+C_2^4A_2+4C_1^2C_2^2A_{1,2}+2\Lambda_1C_1^2B_1+2\Lambda_2C_2^2B_2, \tag{35}$$

where

$$A_j=I_1(L_j), A_{1,2}=\int_{-h/2}^{h/2}\int_0^R \rho\Phi^2_{L_1,k_1,n_1}(\rho,z)\Phi^2_{L_2,k_2,n_2}(\rho,z)(\rho)d\rho dz,\quad B_j=I_2(L_j).$$

The coefficients and the energy of the multivortex state can be obtained analytically as

$$C_1=\pm\left(\frac{-\Lambda_1A_2B_1+2\Lambda_2A_{1,2}B_2}{A_1A_2-4A_{1,2}^2}\right)^{1/2},$$

$$C_2=\pm\left(\frac{-\Lambda_2A_1B_2+2\Lambda_1A_{1,2}B_1}{A_1A_2-4A_{1,2}^2}\right)^{1/2}, \tag{36}$$

and inserting these expressions into Eq. (35) leads to the energy of the multivortex state

$$\mathcal{F}=\frac{-\Lambda_1^2A_2B_1^2-\Lambda_2^2A_1B_2^2+4\Lambda_1\Lambda_2A_{1,2}B_1B_2}{A_1A_2-4A_{1,2}^2}. \tag{37}$$

The stability of the vortex states is determined by the usual criterion for a multivariable function: the Hessian matrix consisting of the second derivatives $\partial^2\mathcal{F}/\partial C_1\partial C_2$ must be positive definite.

In Fig. 16 we present the obtained energy levels of the stable multivortex (MV) states (dashed or dotted curves) obtained through the minimization of the free energy function as a function of the magnetic field and the vorticities of the involved eigenfunctions, for a solid cylinder with radius $R=4\xi$, and height $h=2\xi$, placed in vacuum. All (L_1,L_2) MV states approach asymptotically the corresponding L_1 and L_2 GV states (plotted with solid black curves) because in the limits of their stability the superposition factor $A_{1,2}$ from Eq. (35) approaches zero by the orthogonality of the wave functions $\Phi_{L,k,n}$ against different Ls. In Fig. 17 we present the energy spectrum of the

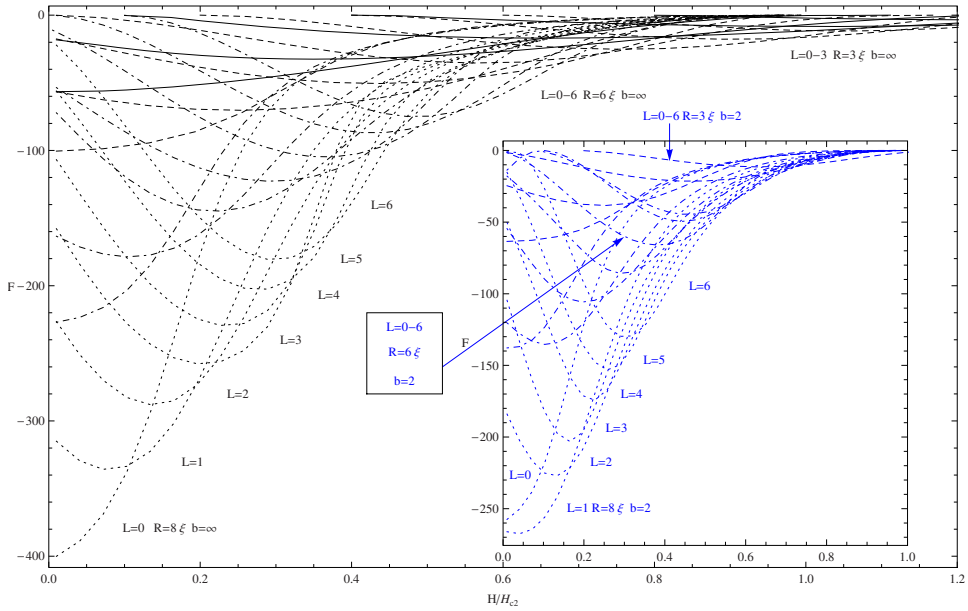

FIG. 14. (Color online) The effect of the radius R on the free-energy curves for giant-vortex states, for vorticities $L=0-6$, for a $h=2\xi$ solid cylinder. The curves represent a cylinder surrounded by vacuum ($b=\infty$) for $R=3\xi$ (solid lines), $R=6\xi$ (dashed lines), and $R=8\xi$ (dotted lines). In the inset we show the same type of dependence, but for a suppressed superconductivity at the surface ($b=2$). The zero-field energy of different sets of curves scales with sample volume.

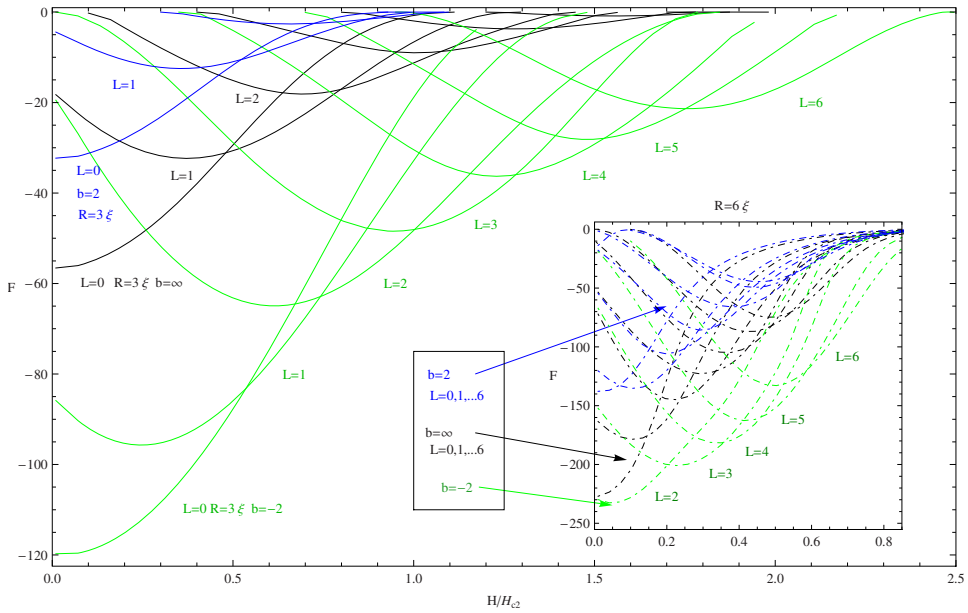

FIG. 15. (Color online) The effect of the surface boundary condition on the dependence $F(H/H_{c_2},L)$ for giant-vortex states of a $R=3\xi$, $h=2\xi$ solid cylinder. The solid lines represent a sample surrounded by vacuum ($L=0,\ldots,5$, $b=\infty$), normal metal ($L=0,\ldots,3$, $b=2$), and higher-T_c superconductor ($L=0,\ldots,6$, $b=-2$). In the inset the dashed lines represent same type of free energy curves, same vorticities, but for a thicker cylinder of radius $R=6\xi$. The influence of the boundary condition at the sample surface on the stability of GV structures (magnetic field ranges) is more intense for thinner cylinders, while for the thicker cylinder practically all GV states collapse close to $H=0.9H_{c_2}$.

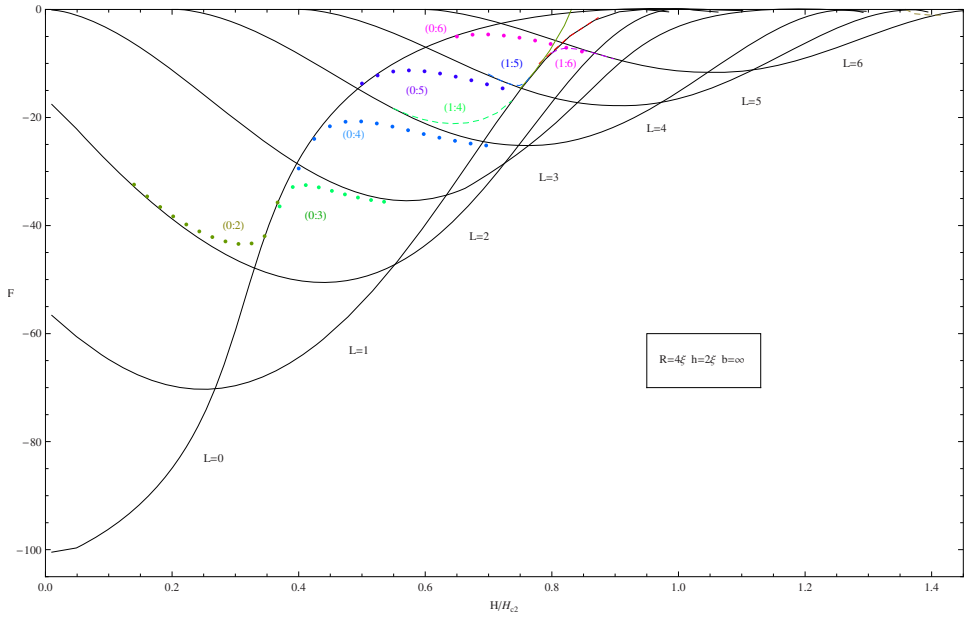

FIG. 16. (Color online) Free energy (for lowest-lying eigenstates $n=k=0$) vs the magnetic field for a superconducting cylinder ($R=4\xi$, $h=2\xi$) in vacuum ($b=\infty$). The solid curves represent giant vortex ($L=0-6$) states, while dotted curves represent multivortex ($L_1:L_2$) states. We assign different line types for different multivortex states, i.e., dotted for $(0:L)$ and dashed for $(1:L)$ states.

vortex states for a wider cylinder with a boundary condition corresponding to suppressing superconductivity (sample surrounded by a normal metal). As a key difference, we note that the multivortex states have the lowest energy in a larger cylinder, whereas this was not generally the case

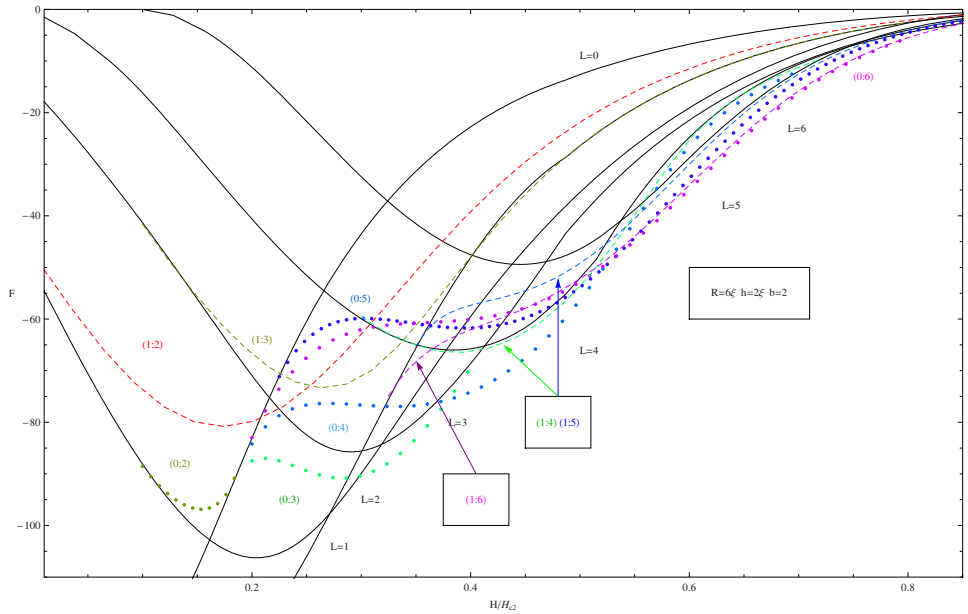

FIG. 17. (Color online) Same analysis as in Fig. 16 but for a wider cylinder ($R=6\xi$, $h=2\xi$) surrounded by superconductivity suppressing material ($b=2$). The solid curves represent GV ($L=0-6$) states, while dotted curves represent $(0:L)$ MV states and dashed curves $(1:L)$ MV states.

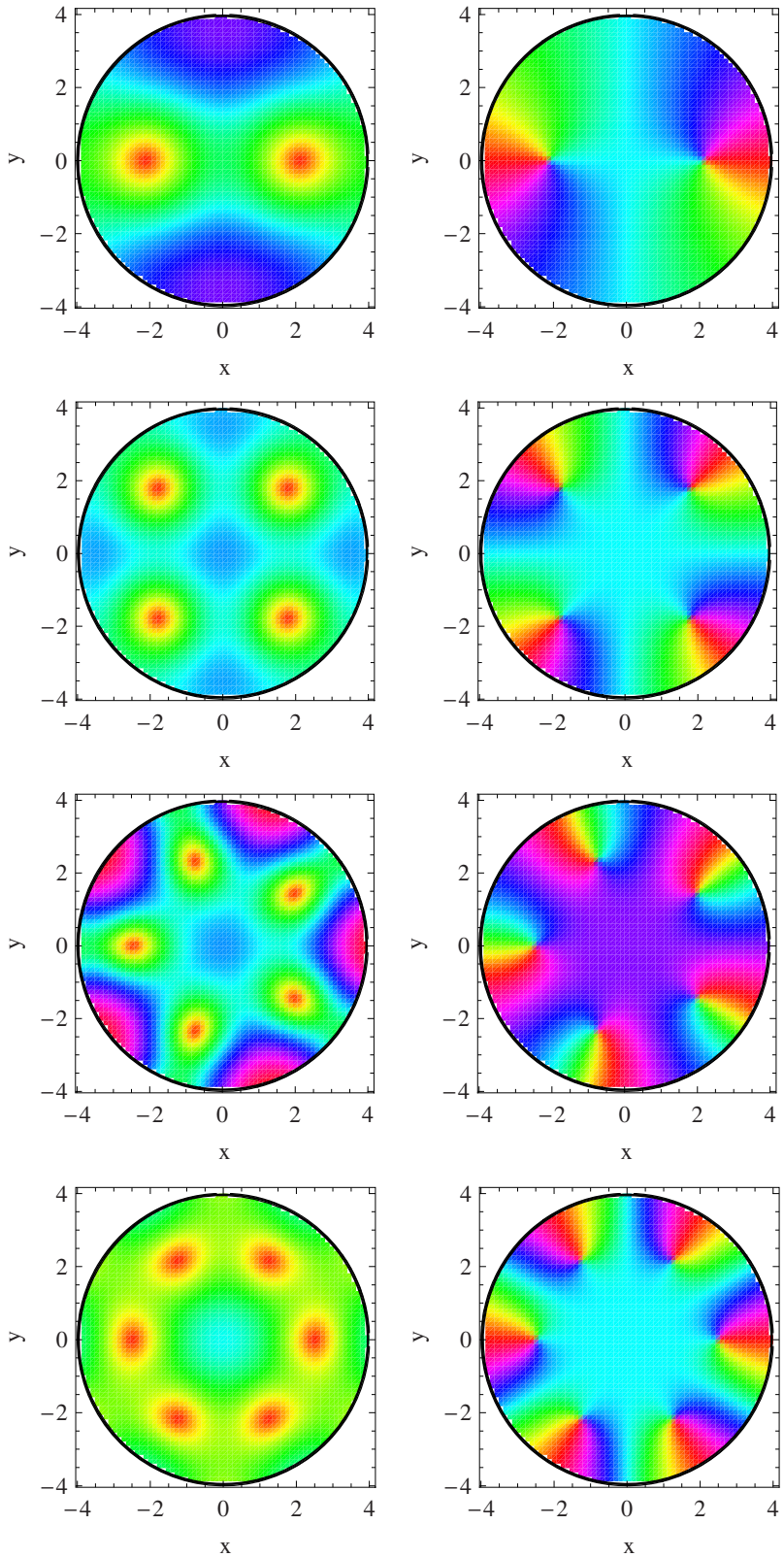

FIG. 18. (Color online) The absolute value of the order parameter $|\Psi(\rho,\varphi,z=0)|$ (top panel) and its phase (bottom panel) for a cylinder with radius $R=4\xi$ and height $h=2\xi$ in vacuum ($b=\infty$). From left to right, we have the following MV states: (0:2) at $H=0.3H_{c2}$, (0:5) at $H=0.55H_{c2}$, (0:6) at $H=0.7H_{c2}$, (1:5) at $H=0.7H_{c2}$, and (1:6) at $H=0.8H_{c2}$. We normalized $|\Psi|$ to 1, and its phase to 2π.

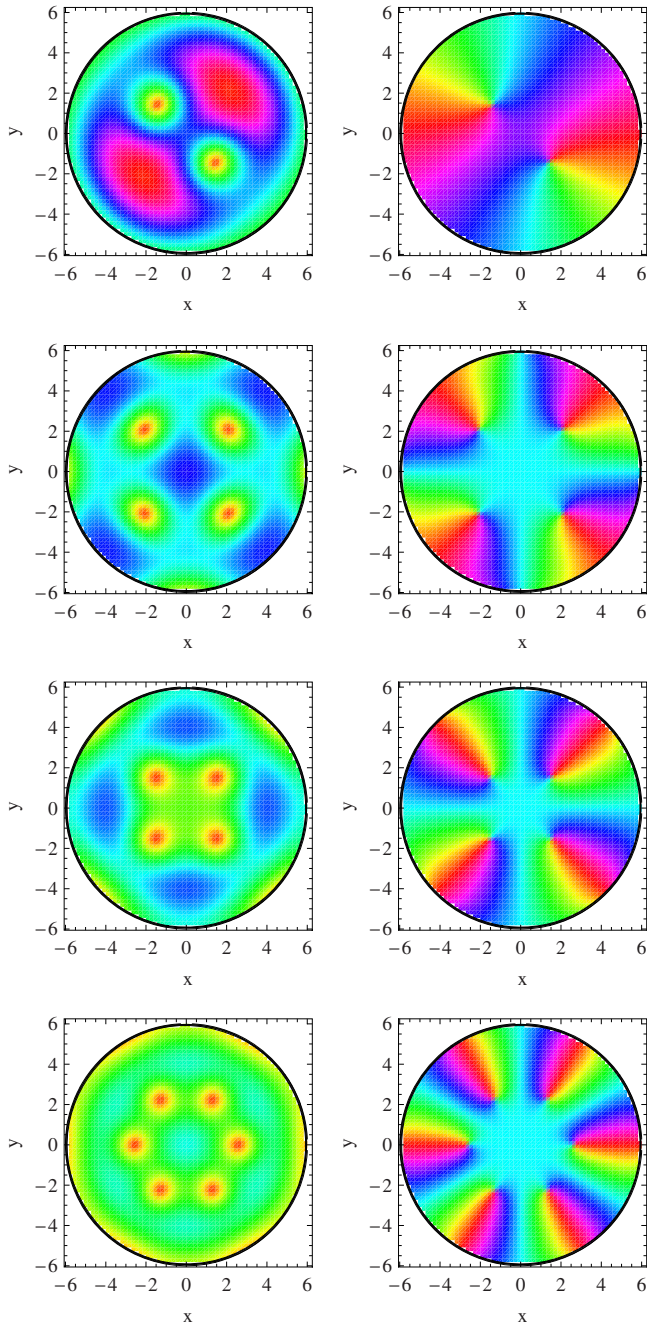

FIG. 19. (Color online) The absolute value of the order parameter $|\Psi(\rho,\varphi,z=0)|$ (top panel) and its phase (bottom panel) for a wider cylinder ($R=6\xi$, $h=2\xi$) placed in a superconductivity suppressing medium $b=2$. From left to right, we show the following MV states: (0:2) at $H=0.3H_{c2}$, (0:4) at $H=0.3H_{c2}$, again (0:4) at higher field $H=0.5H_{c2}$, and (1:6) at $H=0.6H_{c2}$.

in the smaller sample (Fig. 16). Obviously, the increased size of the sample relaxes the vortex confinement, and the splitting of the giant vortex into individual vortices becomes energetically favorable.

To illustrate the multivortex states, we plot in Figs. 18 and 19 the Cooper-pair density, i.e., the absolute value of the MV order parameter function $\psi(\rho,\varphi)$ in a cross section at $z=0$, and in the lowest-lying state ($k=0$, $n=0$), next to the phase of the same order parameter function in the

same plane. In Fig. 18 we present the selected $(0:L)$ and $(1:L)$ multivortex states of a $R=4\xi$ solid cylinder in vacuum for several values of L and H. In Fig. 19 we present the MV states $(L_1:L_2)$ in a cylinder with larger radius where we used a superconductivity suppressing boundary condition. Regarding the vortex positions, we notice that the increased magnetic field compresses the multivortex states to a merger into a giant vortex, as illustrated for the (0:4) state in Fig. 19. The boundary condition in the same figure causes suppression of the order parameter on the sample edges, and shifts the maximum of the encircling Meissner currents toward the interior. This results in a more compact appearance of the MV states compared to Fig. 18. At this point, we also make few general remarks. Namely, our approach leads to the fact that for any stable combination (L_1,L_2) we have a central GV of vorticity $\min\{L_1,L_2\}$, and the remaining number of vortices $|L_2-L_1|$ symmetrically placed around the cylinder axis. Note, however, that the Cooper-pair density plots are not always conclusive with respect to the number and location of vortices in cases when the order parameter is strongly suppressed. This is where the plots of the phase of the order parameter are particularly useful, since the whirling phase change of 2π unambiguously reveals the location of each vortex, and the number of 2π jumps on the contour close to the sample boundary gives the total vorticity in the sample.

VI. MESOSCOPIC SUPERCONDUCTING PERFORATED CYLINDER

Using the same formalism, we study the eigenproblem for hollow cylinders of height h, external radius R_1, and inner radius R_2. In order to use the same type of boundary condition as in the case of a solid cylinder, we need to use both Kummer and Tricomi confluent hypergeometric solutions

$$\Omega_{L,k,n}(\rho)=M\left(\frac{1}{2}-\frac{\Lambda_{L,k,n}-\lambda_k+1}{2H},L+1,\frac{H\rho^2}{2}\right)+CU\left(\frac{1}{2}-\frac{\Lambda_{L,k,n}-\lambda_k+1}{2H},L+1,\frac{H\rho^2}{2}\right) \tag{38}$$

for $R_2\leq\rho\leq R_1$. This radial eigenfunction does not introduce singularities because the origin of the coordinate system is part of the sample. The BC introduces now two equations for $\rho=R_1$ and $\rho=R_2$. On the outer surface $(b_{lat}=b_1)$ we have the usual boundary condition, Eq. (13),

$$\left.\frac{\partial\Omega}{\partial\rho}\right|_{\rho=R_1}=-\frac{\Phi(R_1)}{b_1}, \tag{39}$$

from where we obtain the coefficient C,

$$\begin{aligned}C=-&\left\{(L+1)(2b_1L+2R_1-b_1HR_1^2)M\left(\frac{1}{2}-\frac{\Lambda_{L,k,n}-\lambda_k+1}{2H},L+1,\frac{HR_1^2}{2}\right)\right.\\&\left.+b_1R_1^2(H-\Lambda_{L,k,n}+\lambda_k-1)M\left(\frac{3}{2}-\frac{\Lambda_{L,k,n}-\lambda_k+1}{2H},L+2,\frac{HR_1^2}{2}\right)\right\}\\&\times\left\{(L+1)\left[(2b_1L+2R_1-b_1HR_1^2)U\left(\frac{1}{2}-\frac{\Lambda_{L,k,n}-\lambda_k+1}{2H},L+1,\frac{HR_1^2}{2}\right)\right.\right.\\&\left.\left.-b_1R_1^2(H-\Lambda_{L,k,n}+\lambda_k-1)U\left(\frac{3}{2}-\frac{\Lambda_{L,k,n}-\lambda_k+1}{2H},L+2,\frac{HR_1^2}{2}\right)\right]^{-1}\right\}.\end{aligned} \tag{40}$$

We introduce this value for C in Eq. (38) and by using the inner surface (R_2,b_2) boundary condition [same type of Eq. (13)],

$$\left.\frac{\partial\Omega}{\partial\rho}\right|_{\rho=R_2}=\frac{\Phi(R_2)}{b_2}, \tag{41}$$

we solve it for $\Lambda=\Lambda(R_{1,2},b_{1,2},L,H,k)$. We use again the continued fractions formalism from Sec. IV for the confluent hypergeometric functions, and we obtain an analytical approximation for the

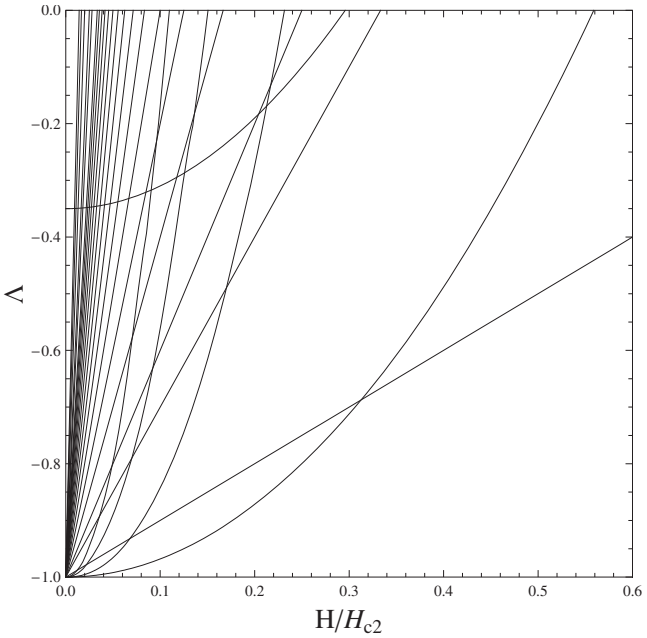

FIG. 20. Eigenvalues Λ for a hollow cylinder $R_1=6\xi$, $R_2=2\xi$, $h=4\xi$ vs magnetic field for several L values. One can note the level crossing between the traditional ground state levels seeded by a solid cylinder $R=6\xi$ and the linear Landau levels.

solutions, which we will not present here because the expression is too large.

The structure of the eigenvalues Λ for the hollow cylinder is similar to the one for a solid cylinder with some extra peculiarities. In addition to the solid cylinder eigenvalues $\Lambda L,k,n(H)$ which are shifted and somehow deformed, we note the existence of some nontraditional eigenvalues Λ identical with the magnetic Landau energies for the same corresponding vorticities. More-

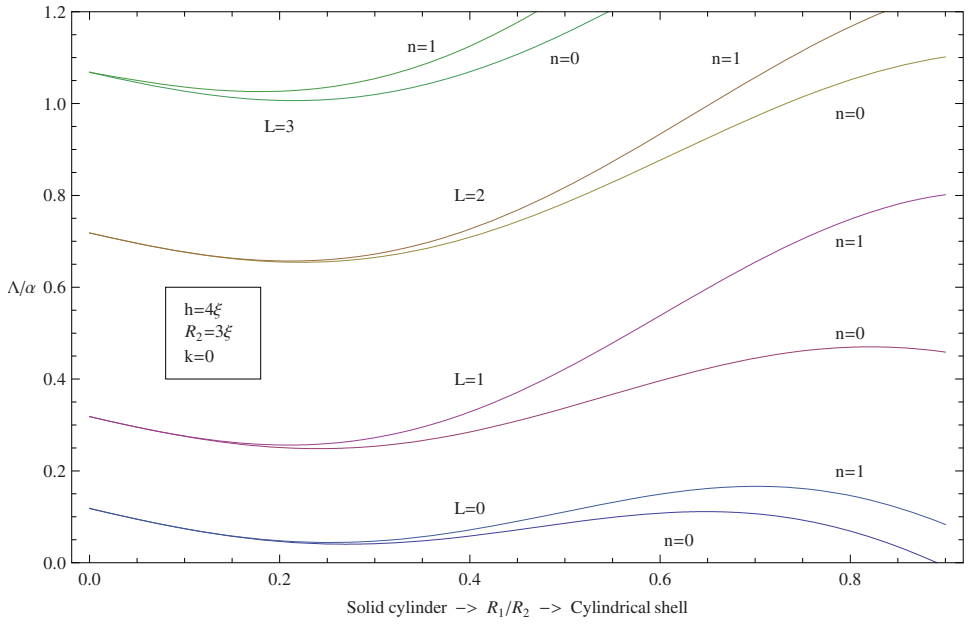

FIG. 21. (Color online) The deformation of the lowest eigenvalues for a cylinder with square vertical cross-section ($h=2R$) for varied radius of the central hole R_2. For $R_2=0$ the spectrum is identical with the spectrum of a solid cylinder, while for larger hole size the spectrum becomes sparser, and splitting of levels is observed.

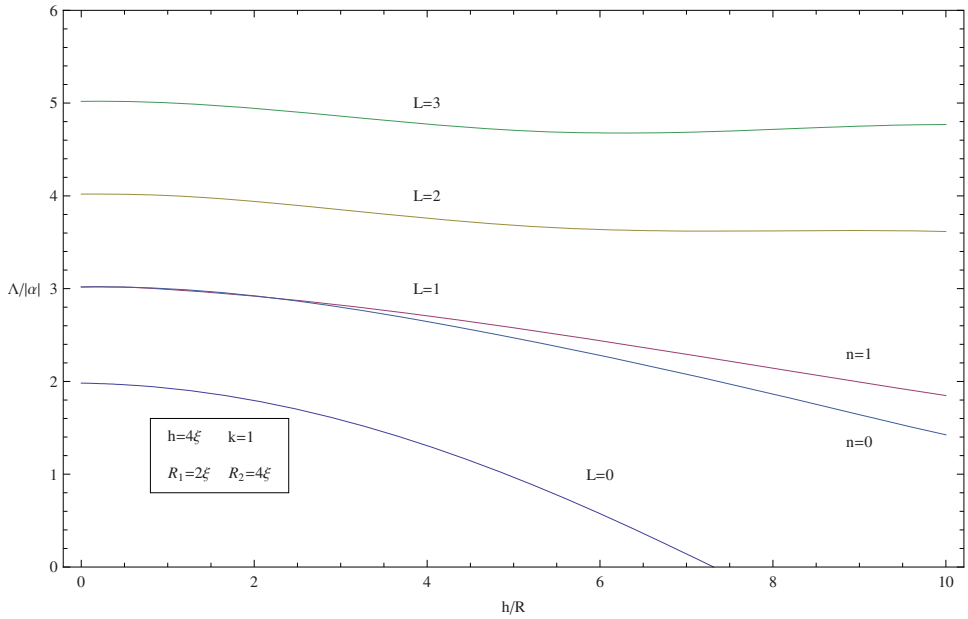

FIG. 22. (Color online) Dependence of the spectrum of a hollow superconducting cylinder as a function of its height.

over, the excited states $n>1$ are more negative values than in case of the solid cylinder case. Consequently, we have level crossing effects for some values of the magnetic field, see Fig. 20, which in principle may induce degeneracy of the ground states. However, when we plot the free energy versus magnetic field and vorticity we do not observe any additional transitions between vortex configurations other than the one predicted by the traditional eigenvalues, because the states associated with these "Landau" levels have much higher free energy.

In order to observe the effect of the size of the hole, we plot in Fig. 21 the eigenvalues for the cylinder with varied radius of the central hole. For small hole radius [punctured cylinder, see Fig. 1(c)] the confluent hypergeometric solutions approach Bessel functions and the spectrum tends to be equidistant—similar to the case of a solid disk (in the limit $R_1 \to 0$). For larger hole [Fig. 1(b)] the levels initially decrease with increasing R_1 and are degenerate for $n=0,1$. When further approaching the limit of a cylindrical shell, the eigenvalues for $n=0,1$ split, the lower eigenvalues become unstable while the higher ones increase further.

In Fig. 22 we present the dependence of the spectrum on the height of a cylinder of radius $R=4\xi$ with a hole of radius $R_1=2\xi$. For $h/R\sim 0$, the spectrum approaches the thin disk case, while for larger height lowest eigenvalues become unstable. Splitting of the degenerate levels with increasing h is observed for $L=1$.

General conclusions can be obtained from this approach relative to the relation between the Λ spectrum and the topology of the boundary. If we integrate the boundary condition in Eq. (11) along Σ we find that the mean value of the order parameter along this boundary is 2π times the Euler–Poincaré characteristic of the domain bounded by Σ. This implies that the multiplicity of the spectrum of a sample with open cavities compared to the spectrum of the whole sample is just given by the number of open cavities performed in the sample. This observation can also be understood by noticing that the cavities introduce actually extra boundary conditions which provide additional zeros of the expression inside the determinant equation (28).

Finally, we construct the actual vortex states of a perforated cylinder, the full solutions to the nonlinear Ginzburg–Landau equation, assuming that the solution for the order parameter can be obtained by an expansion in the basis of just two eigenfunctions of the linear operator. As we did in the Sec. V for the solid cylinder, we first plot the energy levels for different giant and multivortex states in Fig. 23. Here we consider the stability ranges of different states in a hollow cylinder placed in vacuum: the solid-dotted curves of different colors (representing different

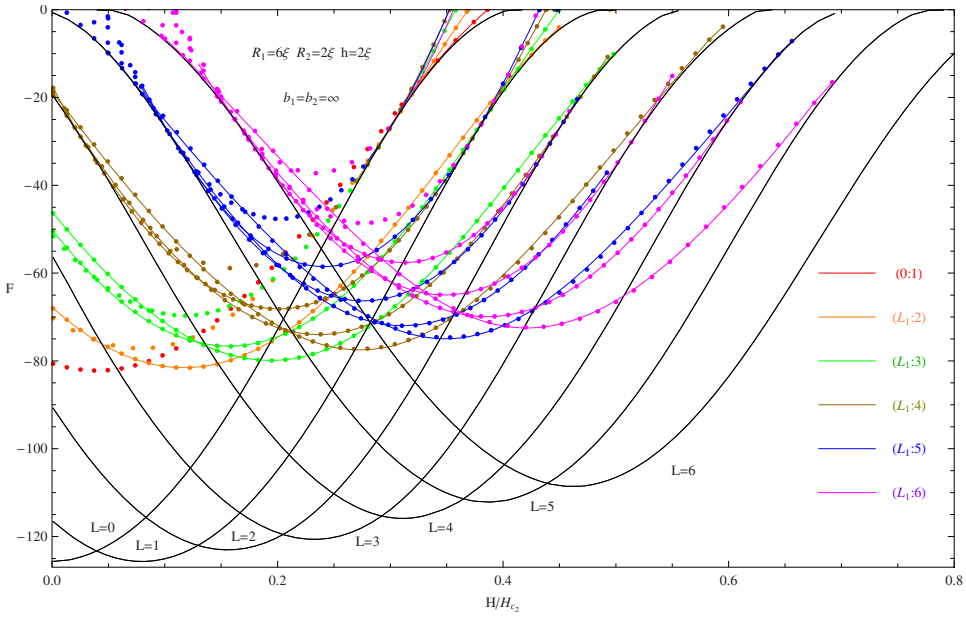

FIG. 23. (Color online) Free energy (for used lowest-lying eigenstates $n=k=0$) for GV and MV states as a function of the magnetic field for a perforated cylinder ($R_1=6\xi$, $R_2=4\xi h=2\xi$) in vacuum ($b=\infty$).

vorticity combinations) are the stable ranges for MV states, while the dotted curves represent the unstable analytical continuations toward their asymptotical GV limits. One distinct feature of a hollow cylinder is the fact that all minima of the free energy in the ground state remain approximately the same, even for different magnetic field and different vorticities. This is a consequence of vortices being trapped by the hole, and therefore weakly affecting the superconducting part of the sample. For the same reason, the stability ranges of the different GV states are very much enhanced compared to the solid cylinder case.

Concerning the multivortex states, the ones with nonzero L_1 are also greatly enhanced compared to the solid cylinder. Generally speaking, a combination of a giant vortex surrounded by individual vortices is not favorable in solid cylinders and disks; instead a full giant or a full multivortex state is realized. Quite the contrary, it is energetically favorable to have this type of states in a perforated cylinder, where a number of vortices are trapped by the hole, and the remaining vortices stay in the superconductor around the perforation. In Fig. 24 we present some examples of these vortex states, as density plots of the absolute value and phase of the order parameter, for a thick cylinder with a narrow cavity $R_1=6\xi$, $R_2=2\xi$.

VII. CONCLUSIONS

In this paper we solved the linear Ginzburg–Landau equation for a superconducting sample with cylindrical shape in a uniform axial magnetic field. We obtained exact analytic expression for the eigenfunctions for boundaries consisting of multiple cylindrical surfaces in terms of a finite sum of confluent hypergeometric functions. As a novelty, the associated eigenvalues are calculated through the expansion of an infinite functional determinant in terms of continued fractions for confluent hypergeometric functions. We analyze the structure of the spectrum in a variety of cases depending on the relative size of the cylindrical surfaces and cylindrical cavities, and on the surface boundary conditions. Among many possible sample geometries (e.g., semispace with finite cylindrical cavity or step, etc.) we demonstrate the method on the solid cylinder case (pillars of different radii) placed in different media. Also, by using the Rayleigh quotient condition of stability for the eigenvalues, we stress the limitations concerning the region in which the superconducting state can exist. Besides being applicable to a variety of superconducting geometries, our

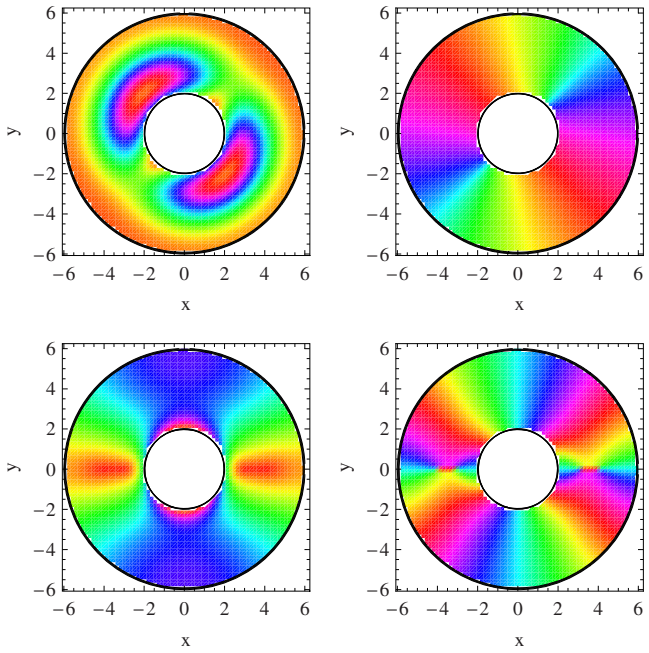

FIG. 24. (Color online) Typical examples of GV and MV states. The density plots for the absolute value of the order parameter are given in the first and third frames, and the phase of the order parameter is shown in the second and fourth frames, for a hollow cylinder $R_1=6\xi$, $R_2=2\xi$, $h=2\xi$, placed in vacuum. The left pair shows a (2:4) state at $H=0.75H_{c2}$ having a double GV inside the hole, with two extra vortices around the perforation. The right pair shows a (3:6) state at $H=0.25H_{c2}$ having a triple GV inside the hole, with three extra vortices around the perforation.

findings facilitate the studies of vortex states deep in the superconducting phase, by solving the full nonlinear Ginzburg–Landau equation using the linear expansion method, as we demonstrated by calculating the energy spectrum and vortex configurations for a solid and perforated cylinder. The method presented in this article allows for more general cylindrical symmetry configurations to be analyzed with high accuracy and time efficiency, like, for example, concentric multilayers of different types of superconducting materials, with open or "blind" axial ends, etc. Moreover, the analytic expressions obtained for the eigenvalues allow to obtain simple expressions for the positions of the centers of the vortices in the given cross section.

[1] C. Sulem and P.-L. Sulem, *The Nonlinear Schrödinger Equation* (Springer-Verlag, Heidelberg, 1999); M. Shifman and A. Yung, Rev. Mod. Phys. **79**, 1139 (2007).
[2] H. Küpfer, G. Linker, G. Ravikumar, Th. Wolf, A. Will, A. A. Zhukov, R. Meier-Hirmer, B. Obst, and H. Wühl, Phys. Rev. B **67**, 064507 (2003); E. T. Filby, A. A. Zhukov, P. A. J. de Groot, M. A. Ghanem, P. N. Bartlett, and V. V. Metlushko, Appl. Phys. Lett. **89**, 092503 (2006).
[3] Ben Xu, M. V. Milošević, and F. M. Peeters, Phys. Rev. B **77**, 144509 (2008).
[4] B. J. Baelus, D. Sun, and F. M. Peeters, Phys. Rev. B **75**, 174523 (2007).
[5] G.-Q. Zha, S.-P. Zhou, B.-H. Zhu, Y.-M. Shi, and H.-W. Zhao, Phys. Rev. B **74**, 024527 (2006); **73**, 104508 (2006).
[6] V. A. Schweigert and F. M. Peeters, Phys. Rev. B **57**, 13817 (1998).
[7] V. A. Schweigert, F. M. Peeters, and P. S. Deo, Phys. Rev. Lett. **81**, 2783 (1998).
[8] A. Kanda, B. J. Baelus, F. M. Peeters, K. Kadowaki, and Y. Ootuka, Phys. Rev. Lett. **93**, 257002 (2004).
[9] S. V. Yampolskii and F. M. Peeters, Phys. Rev. B **62**, 9663 (2000).
[10] B. J. Baelus, S. V. Yampolskii, F. M. Peeters, E. Montevecchi, and J. O. Indekeu, Phys. Rev. B **65**, 024510 (2001).
[11] V. A. Schweigert and F. M. Peeters, Phys. Rev. Lett. **83**, 2409 (1999).
[12] S. Michotte, S. Mátéfi-Tempfli, L. Piraux, D. Y. Vodolazov, and F. M. Peeters, Phys. Rev. B **69**, 094512 (2004); S. Adam, F. de Menten de Horne, L. Piraux, and S. Michotte, Appl. Phys. Lett. **92**, 012516 (2008).
[13] J. J. Palacios, Phys. Rev. Lett. **84**, 1796 (2000); Phys. Rev. B **58**, R5948 (1998).
[14] A. K. Geim, I. V. Grigorieva, S. V. Dubonos, J. G. S. Lok, J. C. Maan, A. E. Filippov, and F. M. Peeters, Nature (London) **390**, 259 (1997).
[15] B. J. Baelus, F. M. Peeters, and V. A. Schweigert, Phys. Rev. B **61**, 9734 (2000).
[16] Y. Chen, M. M. Doria, and F. M. Peeters, Phys. Rev. B **77**, 054511 (2008).
[17] A. Ronveaux, *Heun's Differential Equations* (Oxford University Press, Oxford, 1995).

[18] D. Zwillinger, *Handbook of Differential Equations* (Academic, San Diego, 1998).
[19] G. M. Murphy, *Ordinary Differential Equations and Their Solutions* (Van Nostrand, Princeton, NJ, 1960).
[20] H. L. Cycon, R. G. Froese, W. Kirsch, and B. Simon, *Schrödinger Operators* (Springer-Verlag, Berlin, 1987).
[21] R. Dennemeyer, *Introduction to Partial Differential Equations and Boundary Value Problems* (McGraw-Hill, New York, 1968).
[22] A. M. Hansson, Int. J. Math. Math. Sci. **2005**, 3751 (2005).
[23] L. Erdős, Ann. Inst. Fourier **52**, 1833 (2002).
[24] R. L. Frank, A. Laptev, and S. Molchanov, Proc. Amer. Math. Soc. **136**, 4245 (2008); e-print arXiv:0705.3969 [cond-mat].
[25] L. U. Ancarani and G. Gasaneo, J. Math. Phys. **49**, 063508 (2008).
[26] I. S. Gradshteyn and I. M. Ryzhik, *Table of Integrals, Series, and Products* (Academic, San Diego, 1994).
[27] M. Abramowitz and I. A. Stegun, *Handbook of Mathematical Functions* (National Bureau of Standards, Washington, DC, 1964).
[28] E. Fisher, Proc. Natl. Acad. Sci. U.S.A. **21**, 529 (1935).
[29] G. F. Zharkov, V. G. Zharkov, and A. Yu. Zvetkov, Phys. Rev. B **61**, 12293 (2000).
[30] P. G. de Gennes and J. Matricon, Rev. Mod. Phys. **36**, 45 (1964).
[31] K. Miller and B. Simon, Phys. Rev. Lett. **44**, 1706 (1980).
[32] A. Cuyt, V. Petersen, B. Verdonk, H. Waadeland, and W. B. Jones, *Handbook of Continued Fractions for Special Functions* (Springer, New York, 2008).